Chem Soc Rev

Methane storage in metal–organic frameworks

SCHOLARONE™
Manuscripts

Chem. Soc. Rev.

ARTICLE

Methane storage in metal-organic frameworks

Yabing He,[a] Wei Zhou,[b,c] Guodong Qian,[d] and Banglin Chen[e]*

Natural gas (NG), whose main component is methane, is an attractive fuel for vehicular applications. Realization of safe, cheap and convenient means and materials for high-capacity methane storage can significantly facilitate the implementation of natural gas fuelled vehicles. Physisorption based process involving porous materials offers an efficient storage methodology and the emerging porous metal-organic frameworks have been explored as potential candidates because of their extraordinarily high porosities, and tunable pore/cage sizes and easily immobilized functional sites. In this view, we provide an overview of the current status of metal-organic frameworks for methane storage.

1. Introduction

With the booming development of economy, the demand for crude oil has increased steadily, and as a result concern has risen about the sustainability of oil reserves. Furthermore, the anthropogenic emission of CO_2 from fossil fuel burning in power plants and automobile transport is a growing environmental issue. Considerable efforts have been devoted to develop alternative cleaner fuels to alleviate the pressure on environment and reduce the strong reliance on crude oil. Hydrogen is considered as an ideal clean energy source since no greenhouse gases or other environmentally harmful molecules are released during energy extraction. However, the current technology is still far from commercialization. Natural gas (NG), which mainly consists of methane, is considered as a preferable alternative fuel since it is naturally abundant and relatively environmentally friendly compared to conventional liquid hydrocarbon fuels. It may serve as a bridge fuel to help us through the transition from crude oil to future clean/renewable energy.

Among all hydrocarbons, methane has the highest hydrogen to carbon ratio and consequently the higher research octane number (RON =107), and combustion of methane produces the smallest amount of CO_2 for each unit of heat that is released. However, the relatively low volumetric energy density of methane at normal condition, only 0.11% of that of gasoline, severely exerts constraints on its applications in various possible fields, particularly on-board applications. Therefore, for a large scale usage, it is necessary to develop a safe and efficient technology to obtain a competitive volumetric energy density. Four different methods have been proposed for the storage of natural gas, i.e., Liquefied Natural Gas (LNG), Compressed Natural Gas (CNG), Adsorbed Natural Gas (ANG) and Natural Gas Hydrate (NGH). CNG is stored as supercritical fluid at room temperature and 200-300 bar by using steel cylinder. The main disadvantages of CNG storage are the need for expensive and heavy high pressure storage vessels, costly multistage compression facilities, and potential safety concerns. LNG is obtained by cryogenic techniques and stored as boiled liquid at 112 K and 100 kPa. Even though LNG has high energy density, LNG needs special Dewar containers, and low temperature should be maintained. Moreover, periodic venting is needed because of pressure buildup in a cryogenic fuel tank. NGH is also undesired for practical applications due to the rigorous formation conditions and low formation rate. Besides, the stored gas cannot be released from hydrate just by reducing pressure. ANG technology is a booming technology that combines much lower pressures than those required for CNG and may be achieved at room temperature, unlike liquefaction. This reduction in pressure allows using lightweight, inexpensive, conformable fuel tank, and single stage compressors, and also facilitates at-home refuelling.

Development of efficient adsorbent materials is a key to the success of ANG technology. Many different porous materials have been extensively examined and evaluated as potential methane storage media. The early studies have mainly focused on traditional porous materials such as zeolites, and activated carbons. Despite relatively high packing densities, the low micropore and extreme hydrophilicity of zeolites limit its practical application in methane storage. As for activated carbon, difficulty in tuning pore shapes and sizes has limited the utility. Typically, traditional zeolites exhibit methane uptake below 100 cm^3 (STP) cm^{-3} (standard temperature and pressure equivalent volume of methane *per* volume of the adsorbent material; STP: T = 273.15 K, P = 101.325 kPa), while most porous carbons materials show methane uptake in the range of 50-160 cm^3 (STP) cm^{-3}.[1, 2]

Recently, the Advanced Research Projects Agency–Energy (ARPA-E) of the U.S. Department of Energy (DOE) reset new

methane storage target to guide the research on adsorbent based methane storage.[3] The adsorbent level volumetric energy density needs to exceed 12.5 MJ L^{-1} and 9.2 MJ L^{-1} after packing losses at room temperature. This corresponds to a volumetric storage capacity of 350 cm^3 (STP) cm^{-3} for the adsorbent material. Even if there is no packing loss, the volumetric storage capacity still needs to be higher than 263 cm^3 (STP) cm^{-3}, equivalent to that of CNG at 250 bar and 298 K. The volumetric storage target is significantly higher than the previous one of 180 cm^3 (STP) cm^{-3} at 35 bar.[4] Additionally, DOE sets a target concerning the gravimetric energy density, 0.5 g(CH$_4$) g^{-1}(adsorbent). Accordingly, new porous adsorbents are required to meet these challenging storage targets in order for ANG technology to become practical.

Emerging as a new class of porous materials, metal-organic frameworks (MOFs) have been intensively studied during the past decades. They comprise metal ions or metal containing clusters (generally termed as secondary building blocks (SBUs)) linked by multitopic organic ligands to form 3D networks. A large number of possible organic linkers combined with a plenty of metal ions and metal ion clusters lead to a huge range of potential porous materials with a variety of pore surface properties and chemically tunable structures, which have been assessed for a number of applications including gas storage and separation, catalysis, drug delivery, optical and electronic applications, and sensing.[5-25] For gas storage application, early research on these materials was mostly related to H$_2$. However, the weak interaction between H$_2$ and the surface of MOFs has limited H$_2$ storage to low temperature, typically 77 K. Unlike hydrogen, the interaction energy between methane and the surface of MOFs is already large enough to give reasonable adsorption at room temperature. A growing number of MOFs have been reported for methane storage. Significantly, several MOFs exhibit methane adsorption capacities comparable to or exceeding those of the best activated carbons.

2. Fundaments for ANG storage

2.1 Excess, absolute and total adsorption

In evaluating the methane storage capacities of porous materials, the measurement of adsorption isotherms is a fundamental step. Two different experimental techniques used to measure the amount adsorbed are the volumetric measurement with Sieverts apparatus and the gravimetric method with a microbalance. In reported literatures, the terms such as *excess*, *absolute*, and *total* have frequently been used to describe the gas adsorption capacities.[8, 26] The excess adsorption corresponds to the amount of gas interacting with framework, while the absolute adsorption is the amount of gas both interacting with framework and staying in the adsorbed region in the absence of gas-solid interactions. Total adsorption corresponds to the amount of all gas in the pore. The surface excess adsorbed amount is measured experimentally. Since the experimental techniques applied cannot determine the boundary between adsorbed phase and bulk gas phase, therefore the absolute

adsorption uptake cannot be determined accurately. For gas uptake and delivery purpose, the total adsorbed amount is a more relevant quantity compared to the excess one.

2.2 Gravimetric and volumetric uptakes

Gas adsorption capacities can be expressed in gravimetric or volumetric uptake. Gravimetric uptake is the mass of gas adsorbed per unit mass of adsorbent; while the volumetric one is the volume of gas adsorbed at standard conditions divided by the volume of adsorbent. The volumetric uptake seems to be the most appropriated one to quantify the adsorption capacity of the adsorbents, especially for ANG vehicular application.

Gas adsorption measurement typically gives gravimetric result. In order to calculate the volumetric uptake, a range of different material densities such as crystal density, packing density, densities derived from mercury intrusion porosimetry, have been used. For MOFs, the ideal crystal density has commonly been used to convert gravimetric adsorption capacities to volumetric ones as their crystallographic densities are readily available, representing the ideal maximum storage capacities that MOF materials can generate in practice. The crystallographic density of MOFs is the upper limit of packing density, and cannot be actually achieved for MOF powders. Basically, the low packing density of MOFs may greatly reduce their volumetric storage capacity. Indeed, obvious differences were observed between volumetric uptakes based on the practical packing densities and crystallographic densities for three MOFs.[27] Also, mercury intrusion porosimetry can lead to problems in that the values obtained are strongly dependent on the mercury pressure at which the intrusion is measured. For example, Seki *et al.* used this technique to obtain a density that is even higher than the ideal crystal density.[28]

2.3 Deliverable capacity and storage capacity

A good methane storage material should not only possess a high maximum adsorption capacity but more importantly should have high deliverable capacity. The deliverable capacity, or working capacity, is defined as the amount of gas released when the pressure is reduced. Obviously, the deliverable capacity is less than the storage capacity. On the one hand, the delivered amount depends on the conditions used to trigger the gas release. For example, use of heat or vacuum may trigger much more gas to be desorbed. On the other hand, the deliverable capacity is sensitive to the thermal effects produced due to charge and discharge. If the heat of adsorption released during charge is not removed from the storage system, less methane is adsorbed. If the heat of adsorption is not resupplied during discharge, the residual amount increases. A possible method proposed to address this issue consists of introducing in the adsorbent bed an encapsulated phase change material that has a relatively high heat of fusion at ambient temperature. This material would be capable of adsorbing the heat of adsorption released during charge and resupplying it during discharge.

The volumetric deliverable capacity is more important for improving the driving range of natural gas vehicles (NGVs). For MOFs, the delivery amounts have frequently calculated as

the difference in the amount of methane adsorbed between the upper and lower limiting working pressure at isothermal conditions instead of the practical conditions. Recognizing that a sufficient pressure differential must be provided to drive a sufficient methane flow rate from the adsorbent to the engine, and that a typical working pressure for natural gas powered internal combustion engines is around 5 bar, 5 bar has been taken as the lower limiting working pressure by several groups.[8, 29, 30] A pressure of around 35 or 65 bar is considered the upper limiting working pressure because this can be achieved through a typical single-stage or two-stage compressor. Obviously, to maximize the deliverable capacity of the sorbent, it is necessary to maximize the methane storage at say 65 bar and at the same time minimize the amount of methane stored at around 5 bar.

2.4 Methane/natural gas storage

In most of the ANG studies, methane is used as the test gas to measure the amount of gas stored. However, in actual systems, natural gas, consisting of a complex gas mixture, will be used as a fuel for storage. Consequently, natural gas storage is different from methane storage. The heavy hydrocarbons present in natural gas are preferentially adsorbed upon charging, thus decreasing methane storage capacity. In addition, these components cannot be totally desorbed upon discharging. Therefore, a protective device, i.e., a guard bed, needs to be placed at the adsorbent tank's inlet when storing natural gas in a porous adsorbent. The guard bed removes these compounds and other trace amount of poisonous impurities (H_2S, H_2O, etc.) from the gas stream upon fueling, and then releases these compounds back to the fuel stream using the internal heater.

2.5 Technological requirements

Methane adsorption capacity is not the sole one of the properties that has to be considered in the development of porous materials for ANG applications. Once material meets the storage capacity, the following characters must be considered: (a) quantitative NG desorption under mild conditions, (b) low adsorption heat, (c) high heat capacity, (d) high packing density, (e) high mechanical stability, (f) low affinity for strong adsorbing species, (g) reasonable cost.

Usually, as a common industrial practice, it is essential to compact powdered MOFs into pellets or monoliths under external pressure to increase the packing density. Meanwhile, the textual properties and even the crystal structures might be affected by this compression process. The research on this respect is very limited. Tagliabue *et al.* studied the influence of MOF shaping on physic-chemical characteristics and methane adsorption properties of **CPO-27-Ni**.[31] Compression under 0.1 GPa does not dramatically affect the adsorption kinetics and crystal structure. The obtained tableted MOF exhibits a gravimetric methane adsorption capacity close to that of as synthesized MOF powder. This result is different with those observed for **MOF-5** and **HKUST-1** materials where the compression drastically decreases the gravimetric methane uptake.[29, 32] This different behaviour might be related with the

differences in the mechanical strength. Therefore, for industrial implementation of MOFs as natural gas storage materials, MOFs should have good mechanical properties.

3. Porous MOFs for methane storage

Prior to MOFs, the benchmark materials for methane sorption are activated carbons. In 1997, Kitagawa and co-worker reported for the first time methane sorption on the porous MOF material [Co_2(4,4'-bipyridine)$_3$(NO_3)$_4$] under high pressure.[33] Yaghi's groups in 2002 investigated methane storage capacities of a series of isoreticular MOF materials.[34] After these early reports, there have been some remarkable demonstrations of high methane adsorptions in porous MOFs by various groups. Table 1 summaries the textural properties, and methane storage and working capacities of porous MOFs. In the following section, we will discuss several types of important MOFs for methane storage purposes, with the focus placed on the methane storage mechanism.

3.1 M_2(dicarboxylate)$_2$(dabco)

Studies have shown that pillar-layered MOFs M_2(dicarboxylate)$_2$(dabco) (dabco = 1,4-diazabicyclo[2.2.2]octane) are very promising for methane storage.[27, 28, 35-39] The compounds are composed of dinuclear paddle-wheel units linked by four dicarboxylates into two-dimensional square-grid layers. The axial sites of the paddle-wheels are occupied by nitrogen atoms of the neutral dabco ligands, connecting the 2D layers into a 3D structure with a primitive cubic net topology. Using the short tripod-shaped dabco as a pillar ligand can effectively prevent framework catenation, resulting in noninterpenetrated structures with high porosity. Otherwise, introduction of bidentate pillar linkers longer than dabco will lead to the formation of multiply interpenetrated frameworks.[40] A systematic modulation of dicarboxylate linkers leads to a series of porous isomorphous MOFs with varying size of pores.

Seki *et al.* reported a series of this type of Cu-containing MOFs Cu_2(L)$_2$(dabco) (L = fma, bdc, sdc, or bpdc; fma = fumarate; bdc = benzene-1,4-dicarboxylate; sdc = styrenedicarboxylate; bpdc = biphenyl-4,4'-dicarboxylate), and examined their high-pressure methane adsorption properties.[28, 35, 36] At 298 K and 35 bar, the amount of methane adsorbed increases when pore size increases,. However, two MOF materials Cu_2(bpdc)$_2$(dabco) and Cu_2(sdc)$_2$(dabco) constructed from bpdc and sbc linkers exhibit nearly the same methane uptake, despite that the former has higher porosity than the latter, indicating that the interaction energy of Cu_2(bpdc)$_2$(dabco) for methane is lower than that of Cu_2(sdc)$_2$(dabco) because of larger pore size. This result also means that there exists an optimal pore size in this system for methane adsorption storage. At 298 K and 35 bar, the amounts of methane adsorbed are 212 and 213 cm^3 (STP) g^{-1} for Cu_2(bpdc)$_2$(dabco) and Cu_2(sdc)$_2$(dabco), respectively.

Methane adsorption properties were examined in three isostructural MOFs M_2(bdc)$_2$(dabco) (M= Zn, Cu, Co).[27, 35, 37-39]

This journal is © The Royal Society of Chemistry 2012

Chem. Soc. Rev., 2012, **00**, 1-3 | **3**

Chem. Soc. Rev.

ARTICLE

Table 1. Crystal density, pore volume, surface area and methane adsorption in porous MOFs.[a]

MOF	D_c (g/cm³)	V_p (cm³/g)	BET (m²/g)	Methane adsorption				Methane adsorption				Q_{st} (kJ/mol)	Ref.
				Uptake[b] (cm³/cm³)	Delivery[c] (cm³/cm³)	T (K)	P (bar)	Uptake[b] (cm³/cm³)	Delivery[c] (cm³/cm³)	T (K)	P (bar)		
HKUST-1	0.883	0.78	1850	227	150	298	35	267	190	298	65	17.0	29
HKUST-1	0.881	0.77		225	149	298	35	264	188	298	65	17.0	8
HKUST-1	0.881	0.75	1663	220	141	295	35	259	180	295	65		41
HKUST-1	0.89	0.67	1850	217	152	303	35			303	65		42
HKUST-1	0.88	0.76	1502	198	132	303	35	236	170	303	65		27
HKUST-1	0.881	0.72		197		303	35	234		303	65		43
HKUST-1	0.881	0.71	1555	190		303	35	254		303	65	20.7	44
HKUST extrudates	0.582[e]			94[d]		303	35						45
HKUST-1	0.881	0.73	1587	89[d]		298	18						46
NiMOF-74	1.195	0.56		230	115	298	35	260	142	298	65	20.6	8
NiMOF-74	1.206	0.51	1350	228	106	298	35	251	129	298	65	21.4	29
NiMOF-74	1.206	0.47	1218	214	94	298	35	236	116	298	65		47
NiMOF-74	1.206	0.44	1027	208	100	298	35					20.2	48
PCN-14	0.871	0.87	1753	230		290	35					30	49
PCN-14	0.829	0.83	1984	202	125	298	35	239	160	298	65	17.6	8
PCN-14	0.829	0.85	2000	195	122	298	35	230	157	298	65	18.7	29
CoMOF-74	1.173	0.51		221	110	298	35	249	136	298	65	19.5	8
CoMOF-74	1.169	0.48	1056	193	92	298	35					19.6	48
MgMOF-74	0.909	0.69		200	113	298	35	230	142	298	65	18.5	8
MgMOF-74	0.909	0.63	1542	188	104	298	35	211	127	298	65		47
MgMOF-74	0.909	0.61	1332	168	95	298	35					18.5	48
Zn(bdc)(ted)₀.₅	0.893	0.73	1794	222	168	298	35					15.1	50
Zn₂(bdc)₂(dabco)	0.87	0.75	1448	174		303	35	212		303	65		27
Zn₂(bdc)₂(dabco)	0.826	0.68	1450	160	117	296	35					13.6	37
NJU-Bai10	0.667	1.11	2883	199	107	290	35					14.9	51
NOTT-107	0.756	0.767	1770	196	110	298	35						52
NOTT-109	0.790	0.850	2110	196	125	300	35	242	170	300	65	17.1	30
NOTT-100	0.927	0.677	1661	195	104	300	35	230	139	300	65	18.1	30
UTSA-20	0.910	0.63	1156	195	101	300	35					17.7	53
UTSA-20	0.909	0.66	1620	184	124	298	35	230	170	298	65	18.2	29
PCN-11	0.749	0.91	1931	194	125	298	35	235	166	298	60	14.6	54
NOTT-101	0.684	1.08	2805	194	138	300	35	239	183	300	65	15.5	30
NOTT-103	0.643	1.157	2958	193	140	300	35	236	183	300	65	15.9	30
[Zn₃(OH)]₄(tbcppm) (H₂tbcppm)₂	0.676	1.14	2718	192	146	298	35	275	230[g]	298	65		55
PCN-16	0.724	1.06	2273	191	134	300	35						56
ZJU-5	0.679	1.074	2823	190	130	300	35	228	168	300	65	15.3	57
ZnMOF-74	1.231	0.41	885	188	102	298	35					18.3	48
NU-135	0.751	1.02	2530	187	127	298	35	230	170	298	65	16.6	58
MIL-53(Al)	0.978	0.54	1235	186[d]		303	35						59
MIL-53(Al)	0.978			155[d]		304	35					17	60
NU-125	0.578	1.29	3120	182	133	298	35	232	183	298	65	15.1	29
NU-125	0.578	1.29	3120	181	133	298	35	228	180	298	58	15.5	61
NOTT-102	0.587	1.268	3342	181	136	300	35	237	192	300	65	16.0	30
Cu-TDPAT	0.783	0.93	1938	181	122	298	35	222	163	298	65		62
ZJU-25	0.622	1.183	2124	180	132	300	35	229	181	300	63	15.1	63
ZJU-35	0.657	1.156	2899	177	132	300	35	227	182	300	64		64
IRMOF-6	0.65	0.92		177	134	298	36.5						34
Zn₄O(L1)₂	0.801	0.80	2151	177	117	298	35	213	153	298	65	11.30	65
MnMOF-74	1.084	0.50	1102	176	100	298	35					19.1	48
PCN-46	0.619	1.012	2500	172	132	298	35	206	166	298	65		66
SDU-6	0.611	1.17	2826	172	127	298	35						67
PCN-61	0.56	1.36	3000	171	127	298	35	219	174	298	65		68
UiO-66(Zr)-NH₂	1.36	0.40	1080	166	100	303	35	204	138	303	65		42
Ni(ndc)(ted)₀.₅	0.789	1.34	2307	165	129	298	35					13.8	50

MIL-53(Cr)	1.04			165[d]		304	35					17	[60]
MIL-53(Cr)	1.017			106[d]		304	20						[69]
$Zn_4O(L1\text{-}Cl)_2$	0.839	0.71	1791	164	105	298	35	195	136	298	65	12.55	[65]
$Zn_4O(L1\text{-}CH_3)_2$	0.807	0.75	1908	162	110	298	35	196	144	298	65	11.81	[65]
$Co_2(bdc)_2(dabco)$	0.815	0.82	1600	161	121	303	35	199	159	303	65		[38]
$Co_2(bdc)_2(ted)$	0.847			128[d]		298	36						[39]
NOTT-140	0.677	1.07	2620	159		293	20					16.6	[70]
UTSA-34b	0.840	0.542	991	159	99	290	35						[71]
PMOF-3	0.882	0.718	1840	159	101	298	35						[72]
SDU-7	0.606	1.10	2713	159	114	298	35						[67]
UTSA-40	0.827	0.65	1630	156	102	300	35	192	138	300	65		[73]
MOF-5	0.621	1.4		150	118	298	35	214	182	298	65	12.3	[8]
MOF-5	0.59	1.55	3800	132		298	35						[74]
HNUST-3	0.686	0.99	2412	149		298	20					15.4	[75]
PCN-80	0.574	1.47	3850	147	117	296	35	196	166	296	65		[76]
SDU-8	0.639	1.02	2516	147	105	298	35						[67]
DUT-8(Cu)	0.680	1.04	2535	147	112	298	35	188	153	298	65		[77]
UiO-66(Zr)	1.32	0.36	970	146		303	35						[42]
UiO-67(Zr)	0.708	0.69	1575	146		303	35						[78]
UiO(bpdc)	0.765	1.057	2646	146		293	20					15	[79]
MIL-100(Cr)	0.7	1.10	1900	144	114	303	35	202	172	303	65	19	[80]
MIL-100(Cr)	0.7	0.87	1767	100[d]		298	35						[81]
MIL-100(Cr)	0.7	0.61	1200	55[d]		303	20						[82]
ZJU-36	0.496	1.599	4014	142	114	300	35	203	175	300	65		[64]
MIL-125(Ti)	0.81	0.67	1820	141		303	35						[42]
FJI-H5	0.456	1.92	4255	139	106	298	35	199	166	298	65	10.8	[83]
NU-140	0.426	1.97	4300	138	108	298	35	200	170	298	65	14	[84]
NU-111	0.409	2.09	4930	138	111	298	35	206	179	298	65	15.2	[85]
NU-111	0.409	2.09	4930	138	111	298	35	206	179	298	65	14.2	[29]
PCN-66	0.45	1.63	4000	136	101	298	35	187	152	298	65		[68]
DUT-23(Co)	0.403	2.03	4850	135	112	298	35	197	174	298	65		[86]
MIL-101c(Cr)	0.44	2.15	4230	130	104	303	35	198	172	303	65	18	[80]
MIL-101(Cr)	0.45	1.92	4183	130	106	298	35						[81]
MIL-101(Cr)	0.45	1.57	3870	88	68	303	35	130	110	303	65		[42]
MIL-101(Cr)	0.31	1.303	2693	55	42	303	35	82	69	303	65		[27]
PCN-68	0.38	2.13	5109	128	98	298	35	187	157	298	65		[68]
SNU-50'	0.650	1.08	2300	126		298	35					26.8	[87]
MOF-177	0.43	1.89	4500	126	108	298	35	193	175	298	65		[74]
$Cu(SiF_6)(4,4'\text{-}bpy)_2$	0.859	0.56	1337	125	82	298	36					16.2	[88, 89]
NPC-5	0.822	0.496	1140	124		293	20					16.1	[90]
UTSA-38	0.962	0.61	1090	124[b]		300	35						[91]
$Cu(GeF_6)(4,4'\text{-}bpy)_2$	0.925			124		298	36					16.2	[88]
DUT-4	0.773	0.68	1308	122	82	303	35	164	124	303	65		[92]
MOF-205	0.38	2.16	4460	119	100	298	35	183	164	298	65		[74]
DUT-51(Zr)	0.655	1.08	2335	118	87	298	35	161	130	298	65		[93]
$(Et_2NH_2)_3[(Cu_4Cl)_3(ttca)_8]$	0.736	0.639	1680	118[d]		298	35	145[d]		298	65	18.08	[94]
MIL-100(Fe)	0.7	0.99	2410	117	92	303	35	158	133	303	65		[42]
MIL-100(Fe)	0.7	0.9	1942	88[d]		298	35						[81]
$Zn_4O(bfbpdc)_3(4,4'\text{-}bpy)_{0.5}$	1.054	0.59	1450	116	93	298	35	160	137	298	65		[95]
DUT-5	0.634	0.81	1613	114	94	303	35	134	114	303	65		[92]
IRMOF-8	0.448	1.827	4326	114	71	298	35						[96]
PCN-69	0.355	2.17	3989	114	94	298	35			298	65		[97]
DUT-49	0.309	2.91	5476	112	92	298	35	176	156	298	65		[98]
FJI-1	0.405	1.43	4043	111	90	298	35	164	143	298	65		[99]
PCN-16'	0.764	0.84	1760	111	70	300	35						[56]
$Cu_3(L2)_2(dabco)$	0.603	1.13	2703	111		298	20						[100]
$Cu_4(L3)$	0.706	0.97		111[d]		298	25						[101]
SNU-70'	0.408	2.17	5290	107	91	298	35					9.4	[102]
NOTT-119	0.361	2.35	4118	106	86	298	35	154	134	298	65		[103]
Cd(bpydb)	1.206	0.35	346	105	69	298	35	125	89	298	65		[104]
DUT-6	0.386	2.02		105	89	298	35	163	147	298	65		[105]
MTAF-4	0.670	0.65	1590	105	79	300	35	136	110	298	65		[106]
DUT-9	0.358	2.18		102	83	298	35	155	136	298	65		[107]
NJU-Bai12	0.522	1.135	3038	100		298	20					15.7	[108]
$Zn_4O(fma)_3$	0.812		1120	98[d]		300	28					12.0	[109]
ZJU-32	0.434	1.482	3831	97	77	300	35	140	120	300	60	14.6	[110]
DUT-13	0.385	1.98		96	80	298	35	150	134	298	65		[111]

HNUST-2	0.570	0.97	2366	96		298	20					15.0	[112]
Cu$_3$(tatb)	0.416	1.91	3360	91		273	20						[113]
Cu$_3$(btb)	0.4071	1.77	3288	90		273	20						[113]
SDU-1	0.830	0.353	779	88		293	20					17.6	[90, 114]
Cu(dhbc)$_2$(4,4'-bpy)	1.233			86		298	35						[115]
UTSA-28a-Cu	0.504	1.33	3179	85	65	300	35					16.9	[116]
MOF-210	0.25	3.60	6240	83	71	298	35	143	131	298	65		[74]
Co$_2$(L4)	1.243	0.221	535	80		293	20					16.9	[117]
MIL-96(Al)	1.223			80^d		303	20					16	[118]
Cu$_4$(H$_4$L5)	0.928	0.47		79^d		298	25						[101]
Li$_3$[(Cu$_4$Cl)$_3$(ttca)$_8$]	0.699	0.724	1870	76^d		298	35	85^d		298	65	15.34	[94]
Ni$_3$L$_2$(tpt)$_2$	0.601		1206	71^d		298	35					21.0	[119]
MOF-200	0.22	3.59	4530	67	56	298	35	117	106	298	65		[74]
Cd$_2$(azpy)$_3$(NO$_3$)$_4$	1.539			62	44	298	35					16.33	[120]
Zn$_2$(L6)	1.105	0.155	367	34^b		298	35						[121]
[Cu$_2$(PF$_6$)(NO$_3$)(4,4'-bpy)$_4$]·1.4PF$_6$.0.6NO$_3$	1.057		559	33		298	36					17.0	[88]
Cu$_2$(pzdc)$_2$(pyz)	1.745			31^d		298	31						[122]
SNU-30	0.381	0.28	704	29		298	35						[123]
Cu(Hoxonic)(4,4'-bpy)$_{0.5}$	1.84			21^d		273	25						[124]
SNU-31	0.459	0.14	308	11		298	35						[123]
Cu$_2$(sdc)$_2$(ted)	0.983^f	1.07	3129	(213)^d		298	35						[28]
Cu$_2$(sdc)$_2$(ted)		1.07	3129	(213)^d		298	35					16.48	[36]
Cu$_2$(bpdc)$_2$(ted)		1.18	3265	(213)^d		298	35					16.67	[36]
Cu$_2$(bpdc)$_2$(ted)		1.18	3265	(212)^d		298	35						[28]
MIL-53(Cu)		0.65	1150	(191)^d		298	35						[125]
Cu$_2$(bdc)$_2$(ted)		0.71	1891	(185)^d		298	35					16.25	[36]
Cu(bdc)(ted)$_{0.5}$		0.58	1548	(180)^d		298	35					16.19	[35]
MIL-47(V)		0.5	1030	(143)^d		303	35						[126]
Cu$_2$(fma)$_2$(ted)		0.23	606	(103)^d		298	35					17.04	[36]
Cu(fma)		0.17	416	(82)^d		298	35					15.70	[127]
MIL-96(Cr)				(72)^d		303	20						[82]
Cu(bdc)		0.22	545	(71)^d		298	35					16.96	[127]
Cu(cdc)		0.15	347	(60)^d		298	35					26.57	[127]

^{a} D_c : crystal density; V_p: pore volume; ^{b} Total volumetric uptake; the data in bracket are total gravimetric uptakes; ^{c} The deliverable amount is defined as the difference in total uptake between 5 bar and the specified upper limiting working pressure at isothermal condition; ^{d} Not specified whether uptake is in terms of excess, total or absolute adsorption; ^{e} Real packing density; ^{f} Densities derived from mercury intrusion porosimetry; ^{g} The methane storage capacity of this MOF will need to be carefully and thoroughly re-evaluated independently by other groups; bdc = 1,4-benzenedicarboxylate; ted = triethylenediamine; dabco = 1,4-diazabicyclo[2.2.2]octane; tbcppm = tetrakis{3,5-bis[(4-carboxyl)phenyl]phenyl}methane; tdpat = 2,4,6-tris(3,5-dicarboxylphenylamino)-1,3,5-triazine; H$_3$L1 = 4-[N,N-bis(4-methylbenzoic acid)amino]benzoic acid; H$_3$L1-Cl = 4-[N,N-bis(4-methylbenzoic acid)amino]-2-chlorobenzoic acid; H$_3$L1-CH$_3$ = 4-[N,N-bis(4-methylbenzoic acid)amino]-2-methylbenzoic acid; ndc = naphthalenedicarboxylate; 4,4'-bpy = 4,4'-bipyridine; H$_3$ttca = triphenylene-2,6,10-tricarboxylic acid; H$_2$bfbpdc = 2,2'-bis-trifluoromethyl-biphenyl-4,4'-dicarboxylic acid; H$_3$L2 = [1,1':3',1''-terphenyl]-4,4',5'-tricarboxylic acid; H$_8$L3 = 5,5',5'',5'''-[1,2,4,5-phenyltetramethoxy]tetraisophthalic acid; H$_2$bpydb = 4,4'-(4,4'-bipyridine-2,6-diyl)dibenzoic acid; fma = fumarate; tatb = 5,5',5''-[1,3,5-triazine-2,4,6-triyl-tris(benzene-4,1-diyl)-tris(carbonylimino)]tris-1,3-benzenedicarboxylic acid; btb = 5,5',5''-[benzene-1,3,5-triyl-tris(benzene-4,1-diyl)-tris(carbonylimino)]tris-1,3-benzenedicarboxylic acid; Hdhbc = 2,5-dihydroxybenzoic acid; H$_4$L4 = 2,2',2'',2'''-(2,4,6-trimethyl-1,3-phenylene)bis(methylene)bis(azanetriyl)tetraacetic acid; H$_{12}$L5 = 5,5',5'',5''',5'''',5'''''-[1,2,3,4,5,6-phenylhexamethoxy]hexaisophthalic acid; tpt = 2,4,6-tris(4-pyridyl)-1,3,5-triazine; azpy = 4,4'-azopyridine; H$_4$L6 = tetrakis[4-(carboxyphenyl)oxamethyl]methane acid; pzdc = pyrazine-2,3-dicarboxylate; pyz = pyrazine; H$_3$oxonic = 4,6-dihydroxy-1,3,5-triazine-2-carboxylic acid; sdc = styrenedicarboxylate; bpdc = 2,2'-bipyridine-5,5'-dicarboxylate; cdc = *trans*-1,4-cyclohexanedicarboxylate.

Guest dependent dynamic behavior has been observed in Zn and Co-based MOFs but not in Cu-based MOF.[38, 128] The framework shrinks upon guest inclusion and expands upon guest release. Different methane uptakes of each MOF were reported by different groups. At room temperature and 35 bar, excess methane uptakes of 12.2% and 12.5% were reported by kim[37] and Senkovska,[27] respectively, for Zn based MOF, while excess methane uptakes of 12.2% and 10.8% were reported by Wang[38] and Zhu,[39] respectively, for Co based MOF. Due to no existence of open coordination sites in this system, it is reasonably expected that the different metal center has little effect on methane storage. Therefore, such a discrepancy in methane uptakes should be mainly originated from the sample quality and/or the degree of activation, indicating the significance of the synthesis and activation procedure. Another set of isostructural MOFs M$_2$(2,6-ndc)$_2$(dabco) (M = Ni, Co, Zn, Cu; 2,6-ndc = naphthalene-2,6-dicarboxylate) named as **DUT-8 (M)** with different metal nodes were synthesized by Kaskel *et al.*[77] PXRD and gas adsorption experiments indicated these MOFs exhibited significantly different structural flexibility, depending on the metal ions comprising the nodes. Upon removal and adsorption of guest molecules, **DUT-8(Cu)** remained intact, **DUT-8(Ni)** and **DUT-8(Co)** showed reversible structural transformation, while **DUT-8(Zn)** exhibited irreversible one. Within the **DUT-8** series, **DUT-8(Cu)** has the highest surface area and pore volume as a result of the rigid framework, leading to the highest methane uptake. At 298 K, the methane uptakes of **DUT-8(Cu)** reached 147 and 188 cm^3
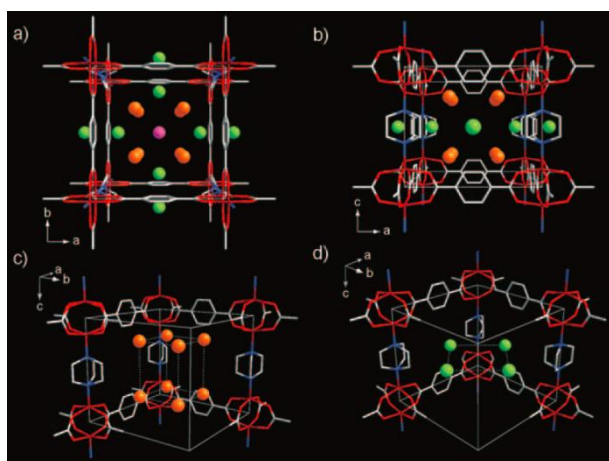
Figure 1. X-ray crystal structure of methane-adsorbed [Zn₂(bdc)₂(dabco)] showing three methane sorption sites (site I: orange, site II: green, site III: purple). Reprinted with permission from ref. [37]. Copyright 2009, Wiley.

(STP) cm^{-3} at 35 bar and 65 bar, respectively.[77]

Kim *et al.* investigated methane binding sites in Zn based MOF compound Zn₂(bdc)₂(dabco) at low temperature.[37] X-ray structure analysis of methane adsorbed sample by synchrotron radiation at 90 K revealed three independent methane sorption sites (Fig. 1). Two primary adsorption sites are near the Zn₂(COO)₄ paddlewheel units (site I), and the center of the small windows along the *a* and *b* axis (site II), respectively. The center of cavity (site III) is a secondary sorption site. Methane molecules located in site I interact not only with the paddlewheel units in van der Waals contact but also with the phenyl rings of the bdc linker through π¨H-C interaction. Methane molecules occupying in site II interact with the side of the phenyl rings through van der Waals interaction. Methane molecules occupying site III are in van der Waals contact with those in sites I and II. Full saturation of these three adsorption sites gives a value which is consistent with what is measured experimentally.

3.2 Zn₄O-based MOFs

Zn₄O(COO)₆ SBU is one very useful inorganic building blocks for the construction of highly porous MOFs. Combination of this type of SBU with a number of dicarboxylates affords a series of isoreticular MOFs (IRMOFs) whose pore spaces can be systematically tuned by changing the length of the dicarboxylates. The high-pressure methane adsorption properties of three numbers in the IRMOF series (**IRMOFs-1, 3, 6**) have been examined, among which **IRMOF-6** has the highest excess methane uptake of 155 cm^3 (STP) cm^{-3} (240 cm^3 (STP) g^{-1}) at 298 K and 36.5 bar.[34] Such high methane uptake in **IRMOF-6** is attributed to high surface area and the hydrophobic nature of C₂H₄ groups. These promising results prompt Snurr *et al.* to perform computational simulations to evaluate the methane adsorption capacities of many hypothetical IRMOFs. They predict that one specially designed MOF material **IRMOF-993,** based on 9,10-anthracene dicarboxylate linker, performs better than **IRMOF-**

6 in terms of volumetric storage capacity.[129] However, attempts to synthesize this proposed MOF result in an ultramicroporous material **PCN-13** with very limited methane uptakes.[130]

In practice, framework interpenetration might be an obstacle in maximizing the porosity of these IRMOF materials. For example, when an extended organic linker such as 2,6-naphthalenedicarboxylate was used instead of 1,4-benezenedicarboxylate in the original **IRMOF-1**, typical solvothermal synthesis at high temperature afforded an interpenetrated framework. Recently, Feldblyum *et al.* discovered a room temperature synthesis approach that allowed for the synthesis of phase-pure noninterpenetrated **IRMOF-8-RT**, and examined its gas sorption properties.[96] At 298 K and 35 bar, excess methane uptake is 193 cm^3 (STP) g^{-1}, corresponding to a relatively low volumetric uptake of 87 cm^3 (STP) cm^3. Thus, a combination of both linker extension and linker functionalization might be needed to simultaneously maximize both gravimetric and volumetric uptakes.

Using neutron powder diffraction, Wu *et al.* directly determined the methane sorption sites in **IRMOF-1** (**MOF-5**) at low temperature.[131] Methane is preferentially adsorbed at the Zn₄O clusters (the primary adsorption site, termed as "cup site") where methane molecules possess well defined orientations. With increasing methane loading, extra methane molecules occupy ZnO₂ site and hex site (the secondary adsorption sites) and are confined inside the central cavity (Fig. 2). ZnO₂ sites are located above the O-O edge of the ZnO₄ tetrahedra, and hex sites on the top of the benzene ring of the organic linkers. Different from the methane molecules at the primary adsorption site, those adsorbed at the secondary adsorption sites are orientationally disordered, implying a weak interaction between methane and framework. The methane confined inside the central cavity is totally disordered and stabilized by the intermolecular interactions with surrounding methane. Interestingly, lowering temperature below 60 K leads to an rearrangement of the confined methane molecule in the central pores of the framework, and accordingly a structural phase transition in MOF-host lattice (Fig. 2c), which is unusual.

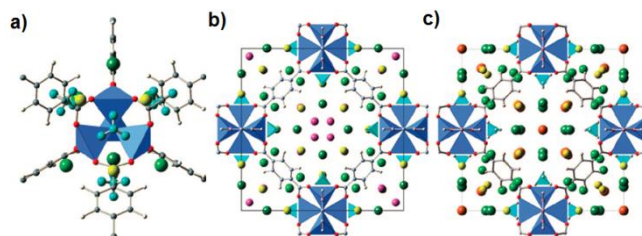However, Raman spectroscopic studies point to the critical

Figure 2. (a) The primary methane adsorption site (cup site, cyan) and the secondary methane adsorption sites (hex site, yellow; ZnO₂ site, green) in **MOF-5**. (b) [001] view of the I4/mmm structure of **MOF-5** with more CD₄ loading at 80 K. Extra methane molecules (pink) were populated near the center of the pores. (c) [001] view of the P4mm structure of **MOF-5** with higher CD₄ loading below 60 K. Confined methane sites (orange) were aligned along the *c* axis and further lowered the symmetry to P4mm. Orientationally disordered methane molecules are shown as spheres for clarity. Reprinted with permission from ref.[131]. Copyright 2009, American Chemical Society.

This journal is © The Royal Society of Chemistry 2012

Chem. Soc. Rev., 2012, **00**, 1-3 | **7**

role that the linkers play in the methane adsorption in IRMOFs at room temperature and high pressure.[132] Upon adsorption, the symmetrical stretching band of methane is downshifted relative to the free methane due to the interaction between methane and the framework. If methane adsorption occurred dominantly at the metal oxide clusters, methane would experience the same frequency shift, independent of IRMOF structures. However, different frequency shifts were observed, revealing that the methane adsorption is dominated by the organic linker at room temperature in these IRMOFs.

Combination of $Zn_4O(COO)_6$ SBU with tricarboxylate linkers yields another class of highly porous MOFs such as **MOF-177**, **MOF-180**, and **MOF-200**.[74, 133] Matzger, Kaskel and Yaghi *et al.* have even been able to assemble two different types of organic carboxylates, namely, triangular tricarboxylate and linear dicarboxylate, leading to a number of exceptionally highly porous noninterpenetrated MOFs. Notable examples include **UMCM-1**,[134] **UMCM-2**,[135] **DUT-6**[105]/**MOF-205**,[74] and **MOF-210**.[74] The framework of the material consists of $Zn_4O(COO)_6$ clusters linked together by 2 dicarboxylate and 4 tricarboxylate linkers arranged in an octahedral geometry. The Langmuir surface area of **MOF-210** is up to 10400 m^2 g^{-1}. Of the Zn_4O-based MOFs reported for methane storage, **MOF-210** has the highest total methane uptake of 476 mg g^{-1} at 298 K and 80 bar. Due to the low framework density, the volumetric methane uptake is quite low.

3.3 MOF-74 series

MMOF-74, also known as **CPO-27-M**, is one of the most well studied families of MOFs bearing the highest concentration of open metal sites reported so far. **ZnMOF-74** was firstly synthesized by Rosi *et al.*[136], and subsequently other analogues were reported.[48, 137-140] Each of these materials is composed of the infinite helical SBUs bound by 2,5-dioxido-1,4-benzenedicarboxylate (DOBDC) to form a 1D honeycomb-like pore structure of ~1.1 nm in diameter. The coordination solvent molecules can be easily removed by thermal treatment under vacuum, resulting in an activated stable framework with a high concentration of coordinatively unsaturated metal sites. These unsaturated metal centers can offer primary binding sites to the guest gas molecules, as has been demonstrated in a number of diffraction studies involving various host-guest combinations.[48, 141-144]

Wu *et al.* compared the methane adsorption properties of the **MMOF-74** series (M = Mg, Mn, Co, Ni, Zn).[48] Their excess adsorption capacities of methane at 298 K and 35 bar range from 149 to 190 cm^3 (STP) cm^{-3}, **NiMOF-74** exhibiting the highest one. All five compounds have very similar heats of adsorption in the range of 18.3-20.2 kJ mol^{-1} at low loading, which is less dependent on the metal identity relative to hydrogen binding energies.[141] This is attributed to the large size and geometrical constraint of methane molecule, increasing the distance between a metal center and a methane molecule, and thereby decreasing interaction potential. Also, the high heat of adsorption results in a rapid increase in the isotherm at low pressure, which is obviously unfavorable to methane delivery.
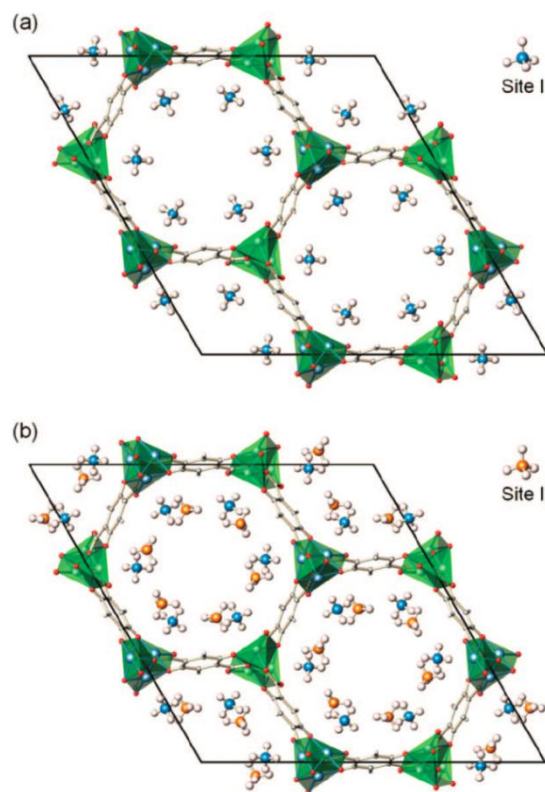

Figure 3. Crystal structure showing (a) the primary adsorption site (site I) and (b) the secondary adsorption site (site II) for methane in **MgMOF-74**. Reprinted with permission from ref.[48]. Copyright 2009, American Chemical Society.

The deliverable amount of methane is less than a half of the storage amount.[145] Dizetzel *et al.* also studied the methane adsorption in **NiMOF-74** and **MgMOF-74**, and the similar results were obtained.[47] Recent studies of Peng[29] and Mason[8] showed a higher methane uptake of about 230 cm^3 (STP) cm^{-3} for **NiMOF-74** at 298 K and 35 bar, again confirming the significance of the sample activation on gas adsorption.

The neutron diffraction experiments clearly indicate that the methane molecules are primarily bound to the open metal sites (site I, Fig. 3a) in the framework through Coulomb interaction.[48] Figure 3b shows a secondary adsorption site (site II) where the methane molecules interact with both the framework and the adjacent methane molecules occupying at the site I. In these MOFs, open metal sites play a major role in the adsorption of methane.

3.4 Copper-carboxylate frameworks
3.4.1 HKUST-1

The well-known material **HKUST-1,** a MOF firstly reported by Chui *et al.*,[146] consists of dicopper paddlewheel SBUs which are connected by 1,3,5-benzenetricarboxylate linkers to form a 3D network containing three different types of cages (Fig. 4a). The small octahedral cage is surrounded by 4 dicopper paddlewheel SBUs and 4 organic linkers with a diameter of approximately 5 Å. The middle cuboctahedral cage of around 10 Å in diameter is encapsulated by 12 dicopper paddlewheel

SBUs and 8 organic linkers, whereas the large cuboctahedral cage of about 11 Å in diameter is constructed from 12 dicopper paddlewheel SBUs and 24 benzenedicarboxylate units. These cages are interconnected at windows. Furthermore, upon removal of the axial water molecules, the copper atoms become coordinatively unsaturated for binding gas molecules. Note that only the large cuboctahedral cage has open copper coordination sites pointing into the pore.

The high-pressure methane adsorption on **HKUST-1** has been widely studied,[8, 27, 29, 43, 147] but inconsistent data were reported by different groups, which was typically due to the sample quality and/or the degree of activation. More recently, Peng *et al.* re-checked the methane adsorption properties of **HKUST-1** and found that it exhibited exceptionally high volumetric methane uptake exceeding any material reported thus far (Fig. 4b).[29] This indicates that optimizing synthesis and activation procedure is very crucial to realize the full potential of MOFs for gas storage. To achieve the high gas uptake, it is necessary to synthesize high-quality phase-pure crystalline sample *via* adjusting the solvothermal reaction conditions, and to optimize carefully the activation profiles including the activation solvent, temperature and time, or to take advantage of the mild activation techniques such as supercritical CO_2 drying,[148] and freeze drying.[149] At 298 K and 35 bar, the total methane uptake is about 230 cm^3 (STP) cm^{-3}. Under higher pressure of 65 bar, **HKUST-1** can reach much higher methane storage capacity up to 267 cm^3 (STP) cm^{-3} at room temperature, which meets the new volumetric target recently set by the U.S. DOE if the packing efficiency loss is ignored. Supposing that 65 bar and 5 bar are taken as the upper and lower limiting pressures for methane delivery, **HKUST-1** also shows excellent deliverable capacity of methane of 190 cm^3 (STP) cm^{-3}.

Kaskel *et al.* investigated the methane adsorption sites in **HKUST-1** at low temperature using high-resolution neutron powder diffraction (NPD).[43] Retiveld analysis of the samples loaded different amounts of CD_4 revealed that methane molecules sequentially occupied distinct adsorption sites, and
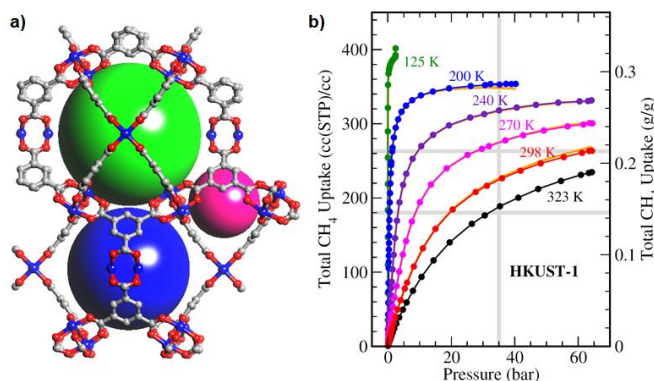
Figure 4. (a) Three different types of cages in **HKUST-1**, and (b) methane adsorption isotherms for **HKUST-1** at various temperatures. The orange color lines represent isotherms obtained from He-cold volume with sample in while the other isotherms are using empty-cell cold volumes. Reprinted with permission from ref. [29]. Copyright 2013, American Chemical Society.
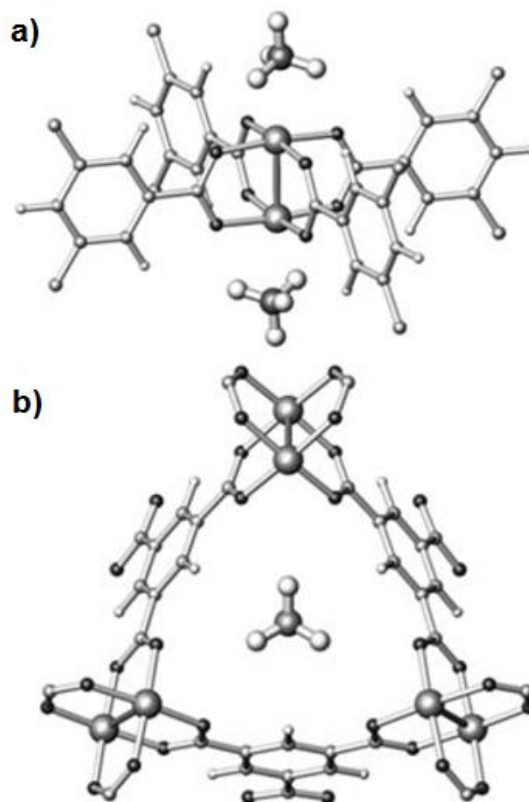
Figure 5. Two primary adsorption sites for methane: (a) open copper site and (b) the small cage window site in **HKUST-1**. Reprinted with permission from ref. [147]. Copyright 2010, Wiley.

more importantly, showed the existence of preferential adsorption sites at the open metal positions for methane. For a sample fully filled with methane molecules, different adsorption sites were unambiguously identified, among which four primary adsorption sites are located inside the pore cages and the windows between the middle and large cages. With decreasing methane loadings, the primary adsorption sites still remain nearly unchanged, but the majority of the methane occupies the large pore cage instead of the small one and open copper sites, which is unexpected considering that the small pore cages and the open metal sites have higher affinity towards methane molecules. The unusual behavior is attributed to the gas adsorption kinetics. During the methane filling process, some adsorbed molecules do not occupy equilibrium sites but are frozen at locations with higher adsorption rate and accessibility.

Zhou *et al.* also performed a comprehensive mechanistic study of methane adsorption in **HKUST-1**.[147] NPD experiments in combination with grand canonical Monte Carlo simulation (GCMC) unambiguously reveal that besides the open copper coordination site, the window site of the small octahedral cage is also one primary methane adsorption site (Fig. 5). These window sites bind methane strongly due to several close interactions in the range of 2.7-3.2 Å between framework O atoms and an adsorbed methane molecule. Moreover, the number of these small cage window sites is equal to 2/3 of that

This journal is © The Royal Society of Chemistry 2012

Chem. Soc. Rev., 2012, **00**, 1-3 | **9**

of the open copper sites. Full saturation of the two primary sites will contribute a methane capacity of around 160 cm^3 (STP) cm^{-3}, which is approximately 70% of the experimental uptake measured at 298 K and 35 bar. The remaining 30% of methane uptake is attributed to the secondary adsorption sites.

Recently, two **HKUST-1** analogues **ZJU-35** and **ZJU-36** were constructed based on less symmetrical tricarboxylates.[64] Significantly, ligand extension enlarges the porosities. At 300 K and 64 bar, the methane uptake capacities of **ZJU-35** and **ZJU-36** reach up to 227 and 203 cm^3 (STP) cm^{-3}, respectively, which are among those of the best MOFs for methane storage.

3.4.2 *NbO*-type copper-tetracarboxylate frameworks

Tetracarboxylates have been widely employed to construct porous framework materials. Chen *et al.* reported the first example of **MOF-505**, which is self-assembled from dicopper paddlewheel SBUs and 3,3',5,5'-biphenyltetracarboxylate, exhibiting high H$_2$ adsorption capacity.[150] Subsequently, a series of tetracarboxylates have been designed and synthesized by several well-known research groups.[49, 54, 58, 87, 151-153] Combination of them and dicopper paddlewheel SBUs usually leads to exceptionally highly porous frameworks. Most of them have (4,4)-connected *NbO*-type structure in which two different types of cages pack alternatively. One is an octahedral cage consisting of 12 ligands and 6 paddlewheel SBUs, while another is a cuboctahedral cage constructed from 6 ligands and 12 paddlewheel SBUs, if the centers of dicopper paddlewheel SBUs are taken as vertexes of polyhedra. These *NbO*-type frameworks have shown excellent framework stability, porosity and gas adsorption capacity.

Wang *et al.* reported a porous *NbO*-type MOF **PCN-11** constructed from dicopper paddlewheel SBUs and a C=C double bond coupled diisophthalate linker, *trans*-stilbene-3,3',5,5'-tetracarboxylate.[54] When the N=N double bond was used as spacer instead of C=C double bond between two isophthalate units, an isostructural but thermally less stable MOF **PCN-10** was formed, leading to its lower porosity. Upon the guest removal, **PCN-11** shows a remarkable total methane uptake of 194 cm^3 (STP) cm^{-3} at 298 K and 35 bar. Due to the high methane uptake capacity, Wu *et al.* employed the NPD experiment and computational simulation to investigate the methane adsorption mechanism in **PCN-11**, and concluded that the open metal sites, the cage window sites and the large cage corner sites provide the major adsorption sites for methane in **PCN-11**.[147]

The same group also synthesized several other *NbO*-type MOFs derived from diisophthalate linkers containing C≡C triple bonds.[56, 66] The assembly of dicopper paddlewheel SBUs and a diisophthalate linker incorporating one C≡C triple bond, 5,5'-(1,2-ethynediyl)bis(1,3-benzenedicarboxylate), under different solvothermal conditions yielded a pair of supermolecular isomers, **PCN-16** and **PCN-16'**, respectively.[56] Despite rather subtle structural difference, the two isomers exhibited significantly different gas adsorption properties. **PCN-16** has a much higher excess methane adsorption capacity

of 175 cm^3 (STP) cm^{-3} at 300 K and 45 bar, compared to just 97 cm^3 (STP) cm^{-3} for **PCN-16'** under the same conditions. The superior gas adsorption properties of **PCN-16** can mainly due to its smaller pore size providing more adsorption sites for methane molecules. Combination of dicopper paddlewheel SBUs and a diisophthalate linker incorporating two C≡C triple bonds, 5,5'-(buta-1,3-diyne-1,4-diyl)diisophthalic acid, *in situ* formed *via* copper catalyzed oxidative coupling of 5-ethylisophthalic acid, gives rise to a porous MOF **PCN-46**.[66] Replacement of phenyl rings by polyyne chain leads to not only a boost of pore volume but also a strong affinity toward gas molecules such as hydrogen and acetylene.[153] The gravimetric excess methane uptake in **PCN-46** reaches saturation at 192 mg g^{-1} at 298 K and 60 bar. At 298 K and 35 bar, the total volumetric methane uptake in **PCN-46** is 172 cm^3 (STP) cm^{-3}.

Shröder *et al.* explored various aromatics rings as spacer between two isophthalates, and constructed a variety of polyphenyl tetracarboxylate linkers, which are incorporated into a series of *NbO*-type frameworks.[151, 152, 154] These desolvated frameworks exhibit high H$_2$ adsorption capacities. Considering the fact that the different densities of open metal sites, and different pore sizes and shapes in these resulting frameworks provide a good chance to systematically investigate the effect of these factors on methane storage and delivery (Fig. 6a), we studied the methane storage and delivery capacities of five representative MOFs: **NOTT-100**, **101**, **102**, **103** and **109**.[30] As shown in Figure 6b, augmentation of pore size from **NOTT-100** to **NOTT-102** results in a decrease in gravimetric methane uptake at low pressure (< 10 bar), indicating that
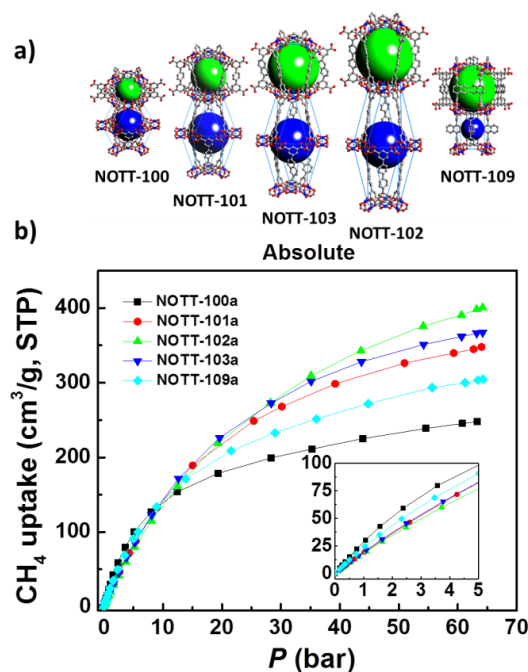

Figure 6. (a) The cage structures and (b) absolute gravimetric high-pressure methane adsorption isotherms at 300 K for **NOTT-100**, **101**, **102**, **103**, and **109**. Inset: an enlargement of the low-pressure region of the sorption isotherms.

methane uptake capacity at low loading is mainly controlled by the methane affinity towards the framework. However, when the pressure goes from 20 bar to 65 bar, the hierarchy of the gravimetric methane uptake capacities is reversed, indicating that the pore volume starts to play a dominant role. At 300 K and 35 bar, they exhibit high volumetric methane adsorption capacities ranging from 181 to 196 cm^3 (STP) cm^{-3}, and excellent methane deliverable capacities in the range of 104-140 cm^3 (STP) cm^{-3}. At 300 K and 65 bar, the volumetric methane adsorption and deliverable capacities are 230 and 139 cm^3 (STP) cm^{-3} for **NOTT-100**, 239 and 183 cm^3 (STP) cm^{-3} for **NOTT-101**, 237 and 192 cm^3 (STP) cm^{-3} for **NOTT-102**, 236 and 183 cm^3 (STP) cm^{-3} for **NOTT-103**, and 242 and 170 cm^3 (STP) cm^{-3} for **NOTT-109**, respectively. Under this condition, the deliverable capacity of **NOTT-102** is comparable to that of **HKUST-1** (190 cm^3 (STP) cm^{-3}).

Ma *et al.* have synthesized a *NbO*-type MOF material called **PCN-14** exhibiting an impressive methane adsorption capacity of 230 cm^3 (STP) cm^{-3} at 290 K and 35 bar,[49] which has been widely cited as one world-record holding MOF materials for methane storage. **PCN-14** is constructed by self-assembly of dicopper paddlewheel SBUs and the organic linker, 5,5'-(9,10-anthracenediyl)diisophthalate. If the centers of dicopper paddlewheel SBUs and the anthracenyl groups are all taken as vertexes of polyhedra, the octahedral cage can be viewed as a squashed cuboctahedral cage in which the anthracenyl rings are in close contact, with the distance of 2.6 Å between a H atom and the center of a phenyl ring from the adjacent anthracenyl group, providing strong van der Waals interaction for methane adsorption; whereas the cuboctahedral cage is regarded to consist of one squashed cuboctahedral cage at the center and two small octahedral cages on the top and bottom (Fig. 7a). Combination of these nanoscopic cages with the open metal sites contributes to its high methane adsorption capacity. The absolute volumetric adsorption capacity of methane in **PCN-14** is up to 230 cm^3 (STP) cm^{-3} at 290 K and 35 bar. Because of the
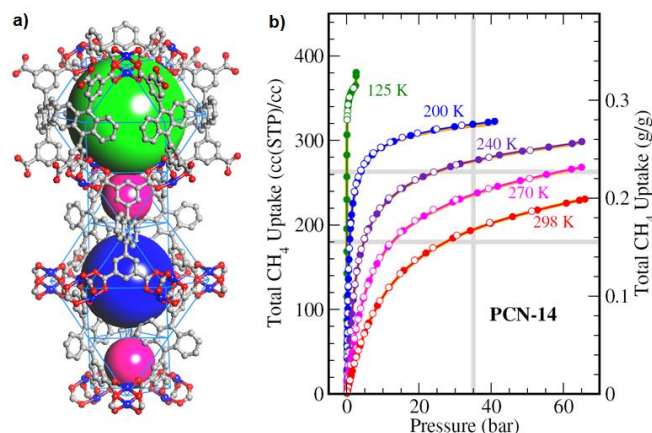
Figure 7. a) Cage structures, and b) high-pressure methane adsorption isotherms in **PCN-14**. The orange color lines represent isotherms obtained from He-cold volume with sample in while the other isotherms are using empty-cell cold volumes. Reprinted with permission from ref.[29] Copyright 2013, American Chemical Society.
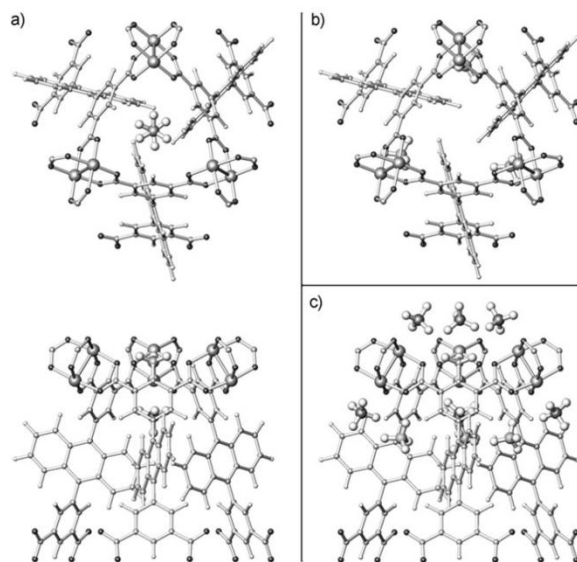

Figure 8. (a) The small cage window site and the small cage bottom site (top and side views), (b) the small cage side window site, and (c) all four major adsorption sites, including the open copper sites in **PCN-14**. Reprinted with permission from ref. [147] Copyright 2010, Wiley.
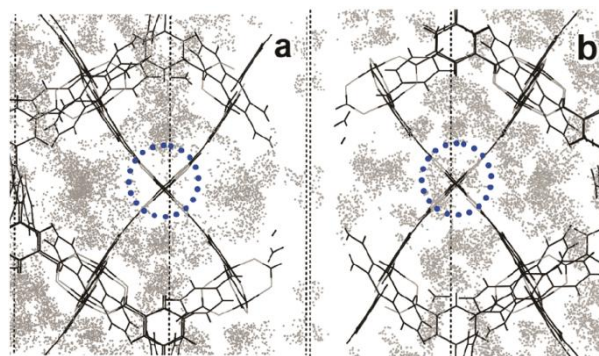

Figure 9. Probability distributions of the centers of mass of methane in **PCN-14** at (a) 3500 kPa and 290 K and (b) 5 kPa and 150 K, viewed along the [211] crystallographic direction. The circles show the probability distributions of the centers of mass of methane molecules in the region where methane molecules are expected to be positioned to populate the open Cu site. Reprinted with permission from ref. [155] Copyright 2008, American Chemical Society.

importance of this benchmark MOF, two groups have re-evaluated the methane adsorption properties of **PCN-14** carefully over a wide range of pressures and temperatures (Fig. 7b).[8,29] The methane uptakes of **PCN-14** were found to be around 195-202 cm^3 (STP) cm^{-3} under 35 bar and 230-239 cm^3 (STP) cm^{-3} under 65 bar at 298 K, once again confirming its high methane storage capacities. The differences among these reports are attributed to slightly different activation conditions, temperatures and framework densities utilized.

Wu *et al.* applied several computational techniques including DFT calculation and GCMC simulations to determine the methane adsorption sites in **PCN-14**.[147] As shown in Figure 8, open copper sites, the small cage windows sites, small cage bottom sites, and small cage side windows sites are the primary adsorption sites. Full occupation of these sites would give 160

This journal is © The Royal Society of Chemistry 2012

Chem. Soc. Rev., 2012, **00**, 1-3 | **11**

cm^3 (STP) cm^3 of methane storage capacity. The remaining storage capacities would be easily provided by the secondary adsorption sites such as large cage corner sites. Interestingly, another simulation study indicates a temperature dependence of open metal site population for methane adsorption. Figure 9 shows probability distributions of the centers of mass of methane at 290 K and 150 K. It can be seen that open copper sites are heavily populated at low temperature, while less populated at room temperature. It was further suggested that there exists no energy barrier between weak and strong sites at room temperature. Open metal sites might play a crucial role in directing methane molecules to other neighboring binding sites.

Molecular simulation identified that a known *NbO*-type MOF, **NOTT-107**, based on 5,5'-(2,3,5,6-tetramethylbenzene-1,4-diyl)diisophthalate linker and dicopper paddlewheel SBUs, is one slightly better methane storage material than **PCN-14**.[52, 152] Absolute methane uptake capacity for **NOTT-107** is predicted to be 213 cm^3 (STP) cm^{-3} at 298 K and 35 bar, but the experimentally measured value is 8% lower than predicted. The authors contribute the discrepancy to incomplete pore activation, reflected by that the experimental surface area is lower than the calculated one. The reason for a high methane uptake in **NOTT-107** is believed to be similar to the one behind **PCN-14**.[49, 147]

By introducing the Lewis basic pyridyl sites into the framework, Rao *et al.* realized a *NbO*-type framework **ZJU-5** exhibiting not only high acetylene storage capacity of 290 cm^3 g^{-1} at 273 K and 1 bar, but also high methane storage capacities of 190 and 228 cm^3 (STP) cm^{-3} under 35 bar and 65 bar at 300 K, respectively.[57] **ZJU-5** is formed by self-assembly of dicopper paddlewheel SBUs and 5,5'-(pyridine-2,5-diyl)diisophthalic acid, in which the isophthalate moieties are coordinated to Cu^{2+} ions to form dicopper paddlewheel SBUs while the pyridyl sites remain unbound. Compared with the analogous MOF **NOTT-101**,[30, 156] **ZJU-5** exhibits a much higher acetylene uptake but a slightly lower methane uptake, indicating that the Lewis basic pyridyl sites might strengthen the interaction with acetylene through pyridyl N···H-C≡C-H hydrogen bonding. The methane storage capacity of **ZJU-5** is still among those of the very few porous MOFs with storage capacities higher than 190 cm^3 (STP) cm^{-3} at room temperature and 35 bar, which is attributed to the interplay of the open copper sites and suitable cage sizes. The same group also synthesized another MOF compound **ZJU-25** with a rare *sty-a* framework topology,[63] which is assembled from dicopper paddlewheel SBUs and a fluorene based diisophthalate, exhibiting a total methane uptake of 180 and 229 cm^3 (STP) cm^{-3} under 35 bar and 63 bar at 300 K, respectively. The deliverable capacity of methane from 63 to 5 bar at 300 K is 181 cm^3 (STP) cm^{-3}, which is among those of a few MOFs with the deliverable capacity of methane higher than 180 cm^3 (STP) cm^{-3} (Table 1).

Incorporation of carborane moiety into the *NbO*-type framework generates a porous *NbO*-type MOF **NU-135**.[58] Interestingly, compared with the analogous terphenyl-based MOF compound **NOTT-101**,[151, 152] **NU-135** has a slightly

reduced pore volume but significantly enhanced volumetric surface area, presumably due to the unique geometrical character of carborane unit, despite the approximately equal length of the linkers employed in two MOFs. Significantly, the interplay between volumetric surface area and pore volume leads to a high methane adsorption capacity. At 298 K, the total methane storage capacities under 35 and 65 bar are 187 and 230 cm^3 (STP) cm^{-3}, respectively. The deliverable amount of methane from 65 to 5 bar at 298 K is 170 cm^3 (STP) cm^{-3}. This study highlights a novel strategy employing a carborane moiety to greatly increase volumetric surface area.

3.4.3 *rht*-type copper-hexacarboxylate frameworks

The traditional strategy for obtaining higher surface area MOFs has been to increase the length of the organic linkers based on a known topology structure. However, extension of the organic linker frequently undermines the framework stability. Upon the removal of guest molecules, the frameworks tend to collapse partially or completely, leading to less porous or even nonporous frameworks. Furthermore, in some cases, undesired framework interpenetration occurs, filling each other's pores. Thus, construction of more stable MOF framework in combination with higher porosity is still a great challenge in the MOF community. In this regard, using metal-organic polyhedra as supermolecular building blocks (SBBs) might be an efficient strategy to construct robust highly porous MOFs. This is because the nano-scale SBBs have intrinsic porosities and higher connectivity compared to the simple SBUs. One widely used SBB is a cuboctahedron, owing to the chemical accessibility of 120°-angular-dicarboxyalte ligands, which is assembled from 12 dinuclear paddlewheel SBUs and 24 isophthalate moieties. Connecting the 24 edges of a cuboctahedron with C_3-symmetrical hexacarboxylate linkers affords a large number of highly porous (3,24)-connected *rht*-type frameworks.[61, 62, 67, 103, 157-165] Notable examples include **NOTT-112**,[159] **PCN-61**,[157] **PCN-66**,[157] **PCN-68**[157]/**NOTT-116**,[161] **PCN-69**[97]/**NOTT-119**,[103] **NU-100**,[166] **NU-111**[160] and **NU-125**.[61] This type of topology was pioneered by Eddaoudi group,[167] and thereafter extensively explored by several other research groups. The use of this type of topology can effectively avoid framework interpenetration, create hierarchical pore cages and generate open metal sites upon desolvation. These features are obviously favorable for high-pressure gas storage.

The structure of these (3,24)-connected *rht*-type MOFs can be viewed as the packing of three different types of polyhedral cage, as illustrated in Figure 10, using **NU-111** as an example. The smallest cage is a cuboctahedron (cub-O_h) composed of 24 isophthalate moieties and 12 dicopper paddlewheel SBUs. The second cage is a truncated tetrahedron (T-T_d) formed by 4 linkers and 12 dicopper paddlewheel units. The largest cage is a truncated cuboctahedron (T-O_h) composed of 8 ligands and 24 dicopper paddlewheel units. One truncated tetrahedron is connected to 4 cuboctahedra, while one truncated octahedron is connected to 6 cuboctahedra, by sharing the triangular and
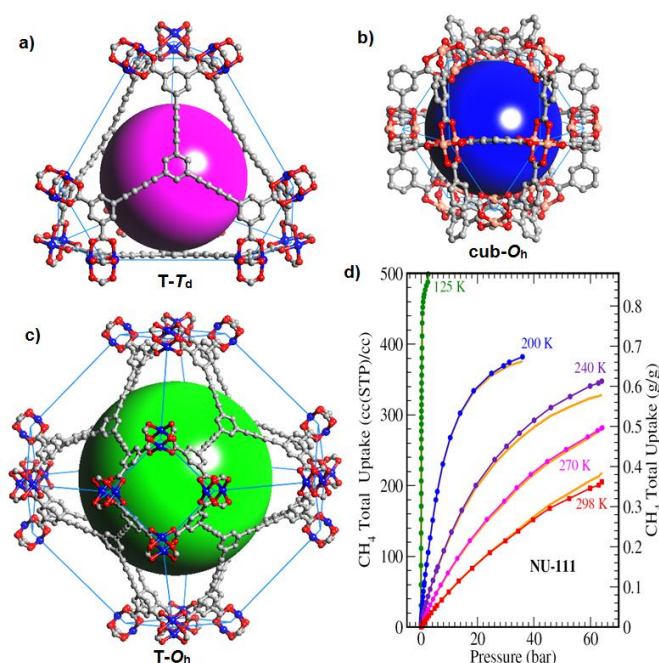
Figure 10. (a-c) Three types of polyhedral cages in **NU-111**: truncated tetrahedron (T-T_d), the cuboctahedron (cub-O_h), and truncated cuboctahedron (T-O_h). (d) High-pressure methane adsorption isotherms of **NU-111** at various temperatures. Reprinted with permission from ref.[29] Copyright 2013, American Chemical Society.

square windows of cuboctahedron, respectively, leading to a highly porous framework.

Yuan *et al.* reported an isoreticular series of (3,24)-connected *rht*-type MOFs **PCN-6x** (x = 1, 6, 8) made from C_3-symmetrical hexatopic ligands incorporating three isophthalates.[157] As expected, the ligand extension enlarges the size of T-O_h and T-T_d but does not change the size of cub-O_h. These MOFs exhibit impressive surface areas and pore volumes. Because gas uptake capacity at low loadings is mainly controlled by the gas affinity towards the framework, as aforementioned, **PCN-61** shows the highest methane uptake capacity in medium pressure range (< 20 bar), which is likely caused by its small pore spaces and high concentration of accessible copper sites. When the pressure goes to high range, the effect of surface area and pore volume starts to dominate, making **PCN-68** the one with the highest methane uptake capacities. The saturated gravimetric methane adsorption capacities correlate well with their gravimetric surface areas/pore volumes. However, the volumetric capacity does not follow the trend due to the different framework density. To achieve high volumetric methane uptake capacity, other factors such as framework density, and pore size, in addition to framework porosity, should be equally taken into account. At 298 K and 35 bar, the volumetric methane uptakes of **PCN-61**, **PCN-66** and **PCN-68** are 171, 136, and 128 cm^3 (STP) cm^{-3}, respectively. At 298 and 65 bar, the adsorption and deliverable capacities of methane are 219 and 174 cm^3 (STP) cm^{-3} for **PCN-61**, 187 and 152 cm^3 (STP) cm^{-3} for **PCN-66**, and 187 and 157 cm^3 (STP) cm^{-3} for **PCN-68**, respectively. Up to 85%

of the storage amount can be delivered, which might be attributed to the hierarchical cage structures.

Hupp and co-workers synthesized a highly porous (3,24)-connected MOF denoted as **NU-111** made from a C_3-symmetrical organic linker whose arm each contains two C≡C triple bond spacers.[160] **NU-111** has a BET surface area of 5000 m^2 g^{-1}, significantly higher than that of **PCN-69/NOTT-119** (3989-4118 m^2 g^{-1}) constructed from a C_3-symmetrical organic linker whose arm each contains two phenyl ring spacers[97, 103], meaning that replacing two phenyl rings in each arm with two triple bonds can greatly boost the molecule-accessible surface area. Based on this strategy, the two MOF materials **NU-109** and **NU-110** have recently been realized, displaying the highest experimental BET surface area of any porous materials reported to date (~7000 m^2 g^{-1}).[168] Most striking feature is that **NU-111** exhibits equally high volumetric and gravimetric methane uptake values (Fig. 10d). The total gravimetric and volumetric uptakes at 298 K and 65 bar reach 0.36 g g^{-1} and 205 cm^3 (STP) cm^{-3}, respectively, which are only 25% lower than the new DOE targets. The deliverable capacity of methane at 298 K from 65 to 5 bar is 177 cm^3 (STP) cm^{-3}.

In choosing MOF materials for methane storage, scale-up synthesis plays equally important roles. Many MOFs do not scale well under the present synthetic pathways, with their purity decreasing at larger reaction sizes. The same groups synthesized in gram scale the other two (3,24)-connected *rht*-type frameworks **NU-125** and **NU-140** based on C_3-symmetrical triazole-based hexacarboxylate linkers, which were easily synthesized *via* click reaction.[61, 84] At 298 K and 65 bar, the volumetric methane adsorption and deliverable capacities are 232 and 183 cm^3 (STP) cm^{-3} for **NU-125**, and 200 and 170 cm^3 (STP) cm^{-3} for **NU-140**.

Zhao *et al.* reported three isostructural (3,24)-connected *rht*-type MOFs (**SDU-6-8**) based on C_3-symmetrical organosilicon-based hexacarboxylates.[67] Interesting, although three isophthalate units on the organic linkers are noncoplanar, the (3,24)-connected *rht*-type network is still formed. More importantly, by changing the functional groups on central silicon atom of the organic linker, the cage size of T-O_h systematically can be tuned, while the sizes of cub-O_h and T-T_d are almost unchanged, thus providing a good chance to see the effect of the functional groups on the gas adsorption capacity. At 298 K and 35 bar, the total volumetric gravimetric methane uptake capacities of **SDU-6-8** are 172, 159, and 147 cm^3 (STP) cm^{-3}, respectively. The higher methane adsorption capacity in **SDU-6** is attributed to its higher surface area and polar hydroxyl groups.

3.4.4 UTSA-20

By immobilizing high density of open metal sites and constructing suitable pore space within a MOF, we realized a porous MOF material **UTSA-20** for high-density methane storage.[53] **UTSA-20** was obtained by a solvothermal assembly of dicopper paddlewheel SBUs and the organic linker H_6bhb (5,5',5''-(benzene-1,3,5-triyl)tris-1,3-benzenedicarboxylic acid).

This journal is © The Royal Society of Chemistry 2012
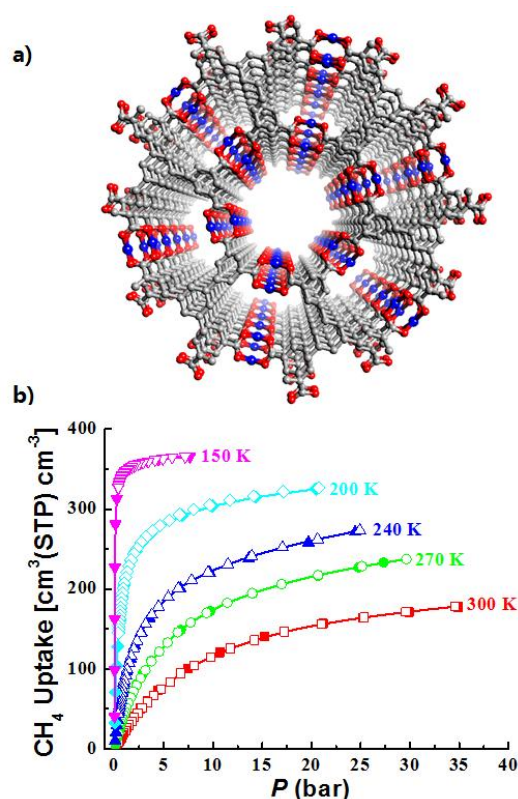
Chem. Soc. Rev., 2012, **00**, 1-3 | **13**

Figure 11. (a) Two types of 1D channels in **UTSA-20**, with open metal sites pointing to the pores, and (b) high pressure methane adsorption isotherms of **UTSA-20**. Reprinted with permission from ref. [53]. Copyright 2011, Wiley.
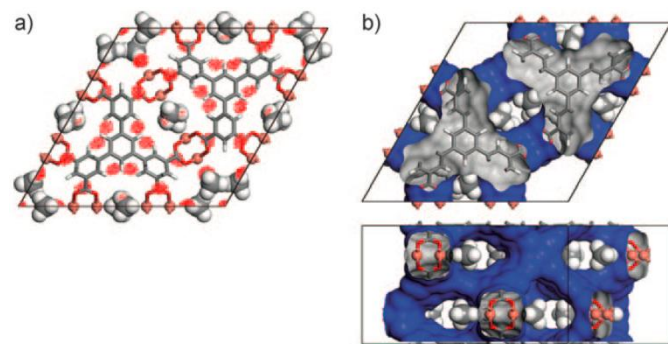
Figure 12. a) Probability distribution of the CH_4 center of mass in **UTSA-20** ([001] view), obtained from GCMC simulation at 298 K and 10 bar. The red regions represent the places where methane molecules are heavily populated in the MOF structure. Note that the open Cu site is preoccupied with CH_4 molecules. b) The pore surface of the interconnected channel pores in UTSA-20 with adsorbed methane at the linker channel site. The channel width along the *c* axis matches well with the size of the adsorbed methane molecules, leading to enhanced van der Waals interaction. Reprinted with permission from ref. [53]. Copyright 2011, Wiley.

There exist 1D rectangular pores of about 3.4 × 4.8 Å and 1D cylinders of 8.5 Å in diameter along the *c* axis, with open metal sites pointing to the pores for binding guest molecules (Fig. 11a). The interplay of the high density of open copper sites and optimal pore spaces enables **UTSA-20** to be a promising material for methane storage. The overall volumetric methane storage capacity is 195 cm^3 (STP) cm^{-3} at 300 K and 35 bar (Fig.

11b). The methane storage density in micropore is 0.222 g cm^{-3}, which is equivalent to the density of compressed methane at 300 K and 340 bar. The methane storage capacity can reach 230 cm^3 (STP) cm^{-3} at 298 K and 65 bar.

Furthermore, GCMC simulation reveals that besides the open copper sites, the channel site is also one primary adsorption site (Fig. 12). Methane binding at linker channel sites is even stronger than that at open metal sites because the methane molecule is well sandwiched between two bhb linker potential surfaces. Full saturation of these two primary sites will generate a methane uptake of 162 cm^3 (STP) cm^{-3}, which is approximately 85% of total methane uptake measured experimentally at 300 K and 35 bar. The remaining 15% of storage capacity can be readily provided by the other secondary binding sites, which exhibit weak interaction with methane.

3.5 MIL series

Férey *et al.* synthesized two zeolite-type mesoporous framework, **MIL-100(Cr)**[169] and **MIL-101(Cr)**,[170] which were built up from trimeric chromium(III) octahedral clusters and trimesate and terephthalate, respectively. In frameworks, two types of mesoporous cages were connected through microporous windows. Because of high porosity and stability, these two MOFs were tested for methane adsorption storage, adsorbing a large amount of methane gravimetrically.[80]

MIL-53 (M = Cr, Al) is a 3D microporous framework containing 1D diamond-shaped channels, which is built from infinite chains of corner sharing $M_4(OH)_2$ octahedra, interconnected by benzenedicarboxylate units.[171] The striking feature is that **MIL-53** exhibits a breathing phenomenon which is triggered by adsorption of polar molecules such as CO_2. In contrast, nonpolar molecules such as methane cannot induce the framework structural transformation due to the lack of a strong specific interaction with the **MIL-53** framework. For methane adsorption at or above ambient temperature, the large pore structure of **MIL-53** is thermodynamically favored over the whole pressure range. The amount adsorbed at 304 K and 35 bar is about 155 cm^3 (STP) cm^{-3} for **MIL-53(Al)** and 165 cm^3 (STP) cm^{-3} for **MIL-53(Cr)**, respectively.[60] Rallapalli *et al.* reported an enhanced methane storage capacity of 186 cm^3 (STP) cm^{-3} for **MIL-53(Al)** using solvent extraction activation method.[59] A Cu-based compound **MIL-53(Cu)** has also been synthesized with methane uptake of 191 cm^3 (STP) g^{-1} at 298 K and 35 bar, but the structure is not still clear.[125]

3.6 Zr-based MOFs

Although some MOFs have exhibited storage capacities which potentially meet or exceed the old DOE target, there are also potential concerns about the stability of these MOFs against the moisture and pressure. Since the discovery of **UiO-66** by Cavka *et al.*,[172] an emerging class of Zr-carboxylate frameworks has attracted great attention in MOF community because high inertness of Zr-carboxylate bonds endows the frameworks with excellent thermal, chemical, and mechanical stability. Numerous isoreticular MOFs such as **UiO-67**, and **UiO-68** have been reported. All these materials are built up from

$Zr_6O_4(OH)_4$ clusters linked by 12 dicarboxylate linkers to form a 12-connected network with *fcu* topology, in which each centric octahedral cage is connected to 8 corner tetrahedral cages through triangular windows.

Yang *et al.* use computational approach to predict the methane adsorption in a series of isoreticular Zr-MOFs, including **UiO-67**, **UiO-68**, Zr-AzoBDC, Zr-AzoBDC and Zr-Cl_2AzoBDC solids.[78] At practical conditions (303 K and 35 bar), **UiO-67(Zr)** shows the highest storage capacity of 146 cm^3 (STP) cm^{-3}. Despite the methane storage capacity is lower than the best performing MOFs such as **HKUST-1**, **PCN-14**, and **UTSA-20**, the high stability against water makes it more attractive for practical methane storage application.

The high degree of connectivity of $Zr_6O_4(OH)_4(COO)_{12}$ gives rise to the high stability but at the same time limits the pore window size and thus negatively effects the availability of pore. Under the premise of ensuring structural stability, reducing the ability of cluster to coordinate multifunctional linker molecules has two beneficial effects: 1) boosting the porosity of MOF material; 2) creating more open metal sites after removal of terminal solvent molecules. Bon *et al.* reported such an example. A porous MOF **DUT-51(Zr)** was made from a bent thiophene dicarboxylate linker, namely dithieno[3,2-b;2',3'-d]-thiophene-2,6-dicarboxylate, using a modulator approach.[93] The Zr-based cluster is 8-connected instead of 12-conneced as reported. The terminal position of cluster is occupied by solvent molecules and modulator molecules, and the terminal solvents can be removed, thus creating open metal sites for binding guest molecules. There exist two distinct types of cages in the framework, namely, octahedron and cuboctahedron, which are connected *via* triangular windows. The maximum excess of methane adsorbed on **DUT-51(Zr)** is 0.12 g g^{-1} at 80 bar and 298 K. More importantly, **DUT-51(Zr)** exhibits high stability against hydrolysis. No significant loss of crystallinity and porosity occurred when the dried sample was immersed in water for 12 h. The high hydrolytic stability is certainly very important for practical application of MOF materials as natural gas adsorbent media in the near future.

An interesting phenomenon observed in **UiO-66(Zr)** is that there exist missing linker defects, which has recently been unambiguously confirmed by Zhou *et al.* using high-resolution NPD technique.[173] By varying the synthesis conditions such as the concentration of the acetic acid modulator and the synthesis time, the linker defects can be tuned systematically. With an increased defect concentration, gas uptake for methane, especially polar CO_2, was enhanced at high pressure. Furthermore, it was found that although the hydrated sample has slightly smaller pore volume and surface area than the dehydrated form, the former performs better than the latter in gas adsorption, which is certainly favorable for practical applications. Such an enhancement effect is attributed to the Columbic interaction between the gas molecules and polar OH groups.

4. Screen, rationalization and optimization of MOFs for methane storage

With the more porous MOFs synthesized and structurally characterized at labs, while reliable instruments for high pressure methane storage studies are kind of limited, it is highly in need to figure out the relationship between the porosity (pore volume or BET surface area) and methane storage capacity of the MOF materials. Thus, we can screen and make the preliminary judgments on their potential for methane storage before some of them can be examined in detail. In this regard, some very promising results have been realized.

He *et al.* examined a series of copper-tetracarboxylate MOFs with similar structures whose porosities are systematically varied for methane storage at room temperature and 35 bar.[30] The study reveals that under this methane storage condition (methane uptakes are still not saturated yet), those porous MOFs with higher porosities (shown both in their higher pore volumes and BET surface areas) have lower methane storage pore occupancies. The pore occupancy, O, under 35 bar and room temperature, is defined as excess methane storage amount under 35 bar and room temperature, C, divided by excess saturated methane storage amount, C_{sat}, which is determined at 150 K. That is reasonable, because the pore spaces within MOFs of large pore volumes are basically larger in dimension than those of small pore volumes, so the larger spaces are less efficiently utilized for methane storage under 35 bar and room temperature. The fact that both the pore occupancy and the excess saturated methane uptake at 150 K are linearly correlated to their pore volume of the porous MOF has enabled to figure out an empirical formula to predict methane storage capacity (under 35 bar and room temperature) of a specific MOF: $C_{excess} = -126.7 \times V_p^2 + 381.6 \times V_p -12.6$; $C_{total} = -126.7 \times V_p^2 + 415.1 \times V_p -12.6$. Here the units of C and V_p are cm^3 (STP) g^{-1} and cm^3 g^{-1} (Fig. 13). Supposing that we know the framework densities from their X-ray crystal structures of the activated samples, we can predict their volumetric storage capacities as well. The calculated methane storage capacities from this empirical formula match quite well with those experimentally determined ones, which will enable us to make a quick judgment on a new porous MOF for its potential application on the methane storage once we characterize its X-ray crystal structure and porosity. It can also help us to evaluate whether or not an optimized activation has been fulfilled for methane storage. Such a simple equation can certainly facilitate our screen of porous MOFs for their methane storage.

Studies on a number of reported porous MOFs by Kong *et al.* revealed that (1/framework density) is linearly correlated to the pore volume of the MOFs, while the total methane uptake at 60 bar and room temperature is linearly dependent on their BET surface area.[64] Accordingly, the total methane storage capacity at 60 bar and room temperature can be approximately calculated based on the following equation: C_{total} (cm^3 (STP) g^{-1}) $= 147.2 + 0.06526 \times BET$ (m^2 g^{-1}).

This journal is © The Royal Society of Chemistry 2012

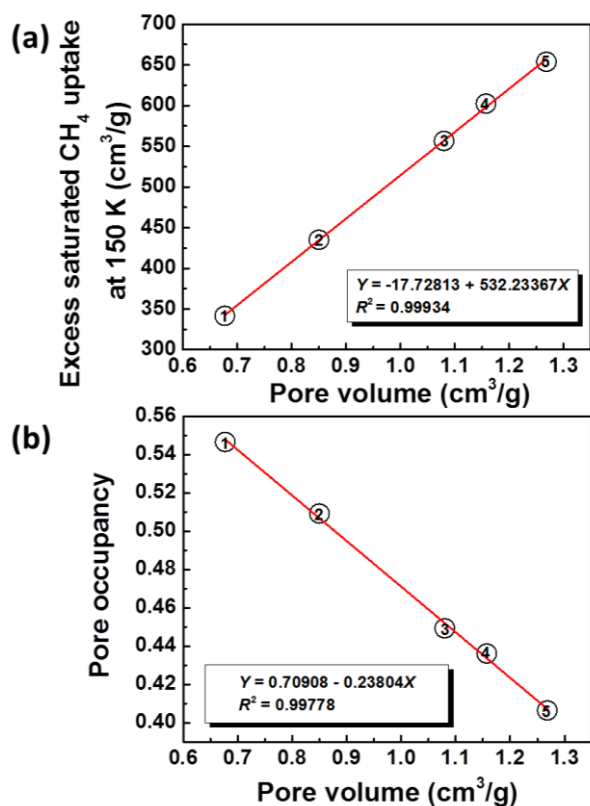*Chem. Soc. Rev.*, 2012, **00**, 1-3 | **15**

Figure 13. (a) Saturated excess gravimetric methane adsorption capacity at 150 K (cm^3 (STP) g^{-1}) versus pore volume (cm^3 g^{-1}) of the MOFs investigated. (b) Pore occupancy versus pore volume (cm^3 g^{-1}). Pore occupancy is defined as the excess gravimetric methane uptake at 300 K and 35 bar divided by the saturated excess gravimetric methane uptake at 150 K. The solid lines show the linear fitting results. 1: **NOTT-100a**; 2: **NOTT-109a**; 3: **NOTT-101a**; 4: **NOTT-103a**; 5: **NOTT-102a**

Figure 14. (a) A schematic diagram showing total gravimetric and volumetric methane adsorption capacities at 298 K and 65 bar, and (b) total gravimetric uptake at 298 K and 65 bar, pore volume, and (1/framework density) as a function of BET surface area in six MOFs: **HKUST-1**, **NiMOF-74**, **PCN-14**, **NU-111**, and **NU-125**. Reprinted with permission from ref. [29]. Copyright 2013, American Chemical Society

Peng *et al.* compared the methane adsorption properties of six promising MOFs (**HKUST-1**, **NiMOF-74**, **PCN-14**, **UTSA-20**, **NU-111**, and **NU-125**) by measuring high pressure isotherms on the same instrument and under the same conditions, leading to reordering of MOF performance ranking.[29] At 298 K and 65 bar, **HKUST-1** and **NU-111** exhibit the best result in terms of volumetric and gravimetric uptake, respectively (Fig. 14a). Furthermore, the pore volume, the gravimetric uptake at 298 K and 65 bar, as well as (1/framework density) are well correlated with BET surface area (Fig. 14b). From these correlations, it can be deduced: 1) total methane storage capacity at 65 bar and room temperature can be approximately calculated based on the equation: C_{total} (cm^3 (STP) g^{-1}) = 0.07958 × BET (m^2 g^{-1}) + 127.1; 2) a hypothetical MOF with BET surface area of 7500 m^2 g^{-1}, pore volume of 3.2 cm^3 g^{-1} and framework density of 0.28 cm^3 g^{-1} can meet the DOE's new gravimetric target of 0.5 g (CH$_4$) g^{-1}(adsorbent).

Although the above mentioned empirical formula can facilitate our screen and target new promising porous MOFs for high methane storage, detailed studies through computational simulations, spectroscopic measurements and diffraction are very important to rationalize the factors and/or parameters and
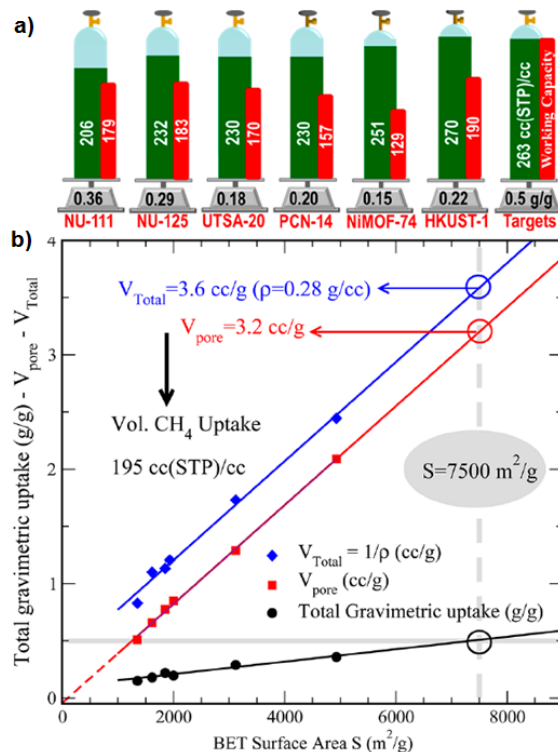
strategies to optimize/maximize methane storage capacities.

Snurr *et al.* used high-throughput computational simulations to predict the textural properties (surface area, pore volume and pore size distribution) and methane uptakes at room temperature and 35 bar in a large number of hypothetical MOFs, and discovered some very useful structure-property relationships.[52] For example, volumetric methane adsorption is proportional to volumetric surface area. In terms of widely used gravimetric surface area, volumetric methane adsorption firstly increases and then begins to decrease when it surpasses the optimal gravimetric surface area of 2500-3000 m^2 g^{-1}. For volumetric methane uptake, the optimal void fraction is around 0.8, and the optimal pore sizes are 4 and 8 Å, exactly big enough for one or two methane molecules. These structure-property relationships provide clues and principles to rationally design MOFs for methane storage.

Raman spectroscopic investigations of methane adsorption behavior in a series of IRMOFs at room temperature and high pressure have revealed that the methane adsorption is dominated by the organic linkers instead of the metal clusters.[132] This result indicates that the linker functionalization may afford a better storage material. Due to the hydrophobic nature of methane, the incorporation of hydrophobic group such as methyl and aromatics groups in the organic linkers might increase methane uptake capacities. In fact, molecular

simulation by Snurr *et al.* has shown that MOFs with lipophilic functional groups such as methyl, ethyl and propyl groups dominate the best performers.[52] In addition, incorporation these hydrophobic groups can improve the moisture stability of the MOFs.

As mentioned previously, Sun *et al.* synthesized three isoreticular *rht*-type MOFs **SDU-6-8** with different function groups immobilized the cuboctahedral cages.[67] The different sizes and surface chemistry of cuboctahedral cages modulated by the functional groups lead to the different methane adsorption capacities. The small and polar OH groups in **SDU-6** enable it to adsorb much more methane at 35 bar. Wang *et al.* investigated the effect of functional groups on methane adsorption properties in three isoreticular microporous MOFs.[65] Their works reveal that introducing functional groups such as CH_3 and Cl increases the heat of adsorption and thus uptake at low pressure, but also reduces the free volume and thus negatively affects the gas adsorption properties at high pressure. Summarizing, the gas sorption properties depend on the positive effect of adsorbate-adsorbent interaction enhancement and the negative effect of the surface area and pore volume reduction upon introduction of functional groups in the framework.

Wu *et al.* determined the exact locations of the stored methane in three MOFs, **HKUST-1**, **PCN-11**, and **PCN-14**, and concluded that open metal sites and van der Waals potential pocket sites are favorable structural features and dominate the methane uptake.[147] The open metal sites are coordinatively unsaturated and can interact favorably with the adsorbate methane through Coulomb interactions, while at the van der Waals pocket sites, the methane molecules interact with multiple surfaces, leading to an overall enhanced dispersive interaction. The design principle has well been demonstrated by Guo *et al.*[53] By immobilization of high density of open metal sites and construction of suitable pore in microporous MOF **UTSA-20**, this MOF exhibits high density of methane storage capacity. In addition, it should bear in mind that pursuing MOFs with high open metal sites will not be a good strategy to target MOFs with high methane delivery.

The doping of MOFs with alkali or transition metals has been used to improve the hydrogen sorption affinities, but this strategy is seldom extended to methane storage. Xiang *et al.* showed that incorporation of CNTs in MOFs can enhance the uptakes of CO_2 and CH_4 by MOFs.[46] The CO_2 and CH_4 adsorption capacities are further improved by doping the CNT modified MOFs with Li^+. It is believed that incorporation of CNT into MOFs increases pore volume while doping MOFs with Li^+ improves the affinity towards gas molecules, thus achieving enhanced composite performance. As for Li doping, the Li^+ content must be maintained at low concentration to achieve the enhancement. Also, Lan *et al.* showed theoretically that doping of COFs with Li^+ ions can significantly enhance the methane uptake of covalent-organic frameworks (COFs).[174] However, Gong *et al.* reported an anionic porous MOF.[94] When counter-cations $Et_2NH_2^+$ were exchanged with Li^+ ions, the methane adsorption capacities were decreased despite the higher pore volume and surface area in Li^+ exchanged MOF. Authors think this is due to the higher affinity of $Et_2NH_2^+$ towards methane than Li^+ ions, which is different to the aforementioned case.

Obviously, methane storage capacities of porous MOFs are dependent on a number of factors. As demonstrated in the empirical formula, the main factor for the gravimetric methane storage amount is still the porosity, which is demonstrated in its pore volume and/or BET surface area. Porous MOFs for high volumetric methane storage need to have balanced porosity and framework density, so the pore space can be efficiently utilized to take up methane molecules. As revealed in several porous MOFs such as **HKUST-1**, **PCN-14** and **UTSA-20** for high volumetric methane storage, those small cages are extremely important for their methane storage; it is highly desirable to design and synthesize porous MOFs with high densities of suitable cages for methane uptakes. As indicated in **MOF-74** series for methane storage, although stronger open metal sites can significantly increase the methane uptakes, their effects on enhancing methane deliverable amounts are quite limited, because these stronger open metal sites also lead to higher methane uptakes under lower pressure of 5 bar. Until now, the effects of some functional organic groups on methane storage are still not very clear, and some more extensive studies through spectroscopic Raman, IR and synchrotron/neutron diffractions are required to target some powerful functional groups/sites for efficient methane storage.

5. Outlook and conclusion

Among the diverse applications of porous MOFs, their applications on methane storage might be the one of the most promising ones. In fact, BASF has commercialized some prototypic MOFs and demonstrated vehicles equipped with natural gas fuel systems containing BASF MOF materials.[175] On the one hand, more scientific studies will be still necessary to target some new porous MOFs for high methane storage; on the other hand, collaboration with industrial partners is very important to enlarge the synthesis and to minimize the cost of the production of MOF materials for their industrial applications. Future works will be even more focused on the methane deliverable amounts instead of methane storage capacities, because the methane deliverable amounts are even more closely related to their practical usage. It is envisioned that some practically useful MOF materials will be eventually implemented in dairy usage for methane storage in the near future.
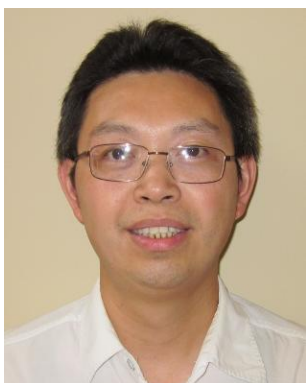
Biographies

Yabing He earned his PhD in organic chemistry from Changchun Institute of Applied Chemistry, Chinese Academy of Sciences, under the direction of Prof. Lianxun Gao in 2010. After that, he worked in the group of Prof. Banglin Chen at University of Texas at San Antonio as a postdoctoral Research Fellow. In 2012, he joined the faculty of Zhejiang Normal University. His current research focuses on the design and synthesis of porous materials and study of their gas adsorption and separation properties.

Wei Zhou received his PhD in 2005 from the University of Pennsylvania, under the supervision of Prof. John E. Fischer. From 2005 to 2007, he was a post-doctoral researcher at the NIST Center for Neutron Research (NCNR), working with Dr. Taner Yildirim. After that, he was appointed to his current position as a research scientist at NCNR and the University of Maryland. His research interests are in the areas of novel porous materials, computational materials design, and neutron spectroscopy.

Guodong Qian was born in Zhejiang, China. He received his bachelor's (1988) and master's (1992) degrees in Materials Science from Zhejiang University in China. He joined the Materials Department of Zhejiang University after obtaining his Ph.D. degree from Zhejiang University in 1997. He was promoted to associate professor, full professor and Cheung Kong professor in 1999, 2002 and 2011, respectively. His current research interests include hybrid organic-inorganic photonic functional materials, cathode or anode materials of lithium-ion batteries, and multifunctional porous materials.

Banglin Chen was born in Zhejiang, China. He received B.S. (1985) and M.S. (1988) degree in Chemistry from Zhejiang University in China, and Ph.D. from National University of Singapore in 2000. He has been working with Professors Omar M. Yaghi at University of Michigan, Stephen Lee at Cornell University and Andrew W. Maverick at Louisiana State University as the postdoctoral fellow during 2000-2003 before joining the University of Texas-Pan American in 2003. He moved to the University of Texas at San Antonio in August 2009, and now he is the Professor of Chemistry.

Notes and references

[a] College of Chemistry and Life Sciences, Zhejiang Normal University, Jinhua 321004, China.
[b] NIST Center for Neutron Research, Gaithersburg, Maryland 20899-6102, USA. E-mail: wzhou@nist.gov
[c] Department of Materials Science and Engineering, University of Maryland, College Park, Maryland 20742, USA.
[d] State Key Laboratory of Silicon Materials, Department of Materials Science & Engineering, Zhejiang University, Hangzhou 310027, China
[e] Department of Chemistry, University of Texas at San Antonio, One UTSA Circle, San Antonio, Texas 78249-0698, USA. Fax: (+1)-210-458-7428; E-mail: banglin.chen@utsa.edu

1. D. Lozano-Castelló, J. Alcañiz-Monge, M. A. d. l. Casa-Lillo, D. Cazorla-Amorós and A. Linares-Solano, *Fuel*, 2002, **81**, 1777-1803.
2. V. C. Menon and S. Komarneni, *J. Porous Mater.*, 1998, **5**, 43-58.
3. See DOE MOVE program at https://arpa-e-foa.energy.gov/.
4. T. Burchell and M. Rogers, *SAE Tech. Pap. Ser.*, 2000, **2000-01-2205**.
5. M. P. Suh, H. J. Park, T. K. Prasad and D.-W. Lim, *Chem. Rev.*, 2012, **112**, 782-835.
6. Y. Yan, S. Yang, A. J. Blake and M. Schröder, *Acc. Chem. Res.*, 2013, 10.1021/ar400049h.
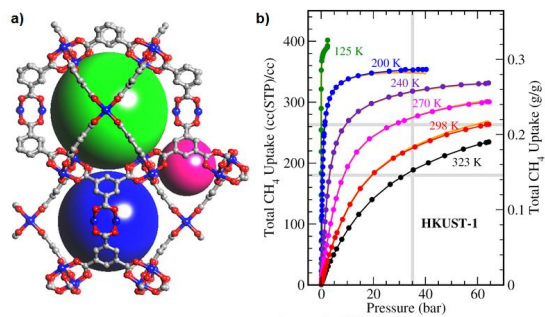
7. T. A. Makal, J.-R. Li, W. Lu and H.-C. Zhou, *Chem. Soc. Rev.*, 2012, **41**, 7761-7779.

8. J. A. Mason, M. Veenstra and J. R. Long, *Chem. Sci.*, 2014, **5**, 32-51.

9. K. Konstas, T. Osl, Y. Yang, M. Batten, N. Burke, A. J. Hill and M. R. Hilla, *J. Mater. Chem.*, 2012, **22**, 16698-16708.

10. W. Zhou, *Chem. Rec.*, 2010, **10**, 200-204.

11. S. Ma and H.-C. Zhou, *Chem. Commun.*, 2010, **46**, 44-53.

12. J.-R. Li, J. Sculley and H.-C. Zhou, *Chem. Rev.*, 2012, **112**, 869-932.

13. J. Lee, O. K. Farha, J. Roberts, K. A. Scheidt, S. T. Nguyen and J. T. Hupp, *Chem. Soc. Rev.*, 2009, **38**, 1450-1459.

14. L. Ma, C. Abney and W. Lin, *Chem. Soc. Rev.*, 2009, **38**, 1248-1256.

15. A. Corma, H. García and F. X. L. i. Xamena, *Chem. Rev.*, 2010, **110**, 4606-4655.

16. G. Nickerl, A. Henschel, R. Grünker, K. Gedrich and S. Kaskel, *Chem. Ing. Tech.*, 2011, **83**, 90-103.

17. Y. Liu, W. Xuan and Y. Cui, *Adv. Mater.*, 2010, **22**, 4112-4135.

18. P. Horcajada, R. Gref, T. Baati, P. K. Allan, G. Maurin, P. Couvreur, G. Férey, R. E. Morris and C. Serre, *Chem. Rev.*, 2012, **112**, 1232-1268.

19. Y. Cui, Y. Yue, G. Qian and B. Chen, *Chem. Rev.*, 2012, **112**, 1126-1162.

20. B. Chen, S. Xiang and G. Qian, *Acc. Chem. Res.*, 2010, **43**, 1115-1124.

21. L. E. Kreno, K. Leong, O. K. Farha, M. Allendorf, R. P. V. Duyne and J. T. Hupp, *Chem. Rev.*, 2012, **112**, 1105-1125.

22. S. Kitagawa, R. Kitaura and S.-i. Noro, *Angew. Chem. Int. Ed.*, 2004, **43**, 2334-2375.

23. H.-L. Jiang and Q. Xu, *Chem. Commun.*, 2011, **47**, 3351-3370.

24. J.-P. Zhang, Y.-B. Zhang, J.-B. Lin and X.-M. Chen, *Chem. Rev.*, 2012, **112**, 1001-1033.

25. H. Wu, Q. Gong, D. H. Olson and J. Li, *Chem. Rev.*, 2012, **112**, 836-868.

26. W. Zhou, H. Wu, M. R. Hartman and T. Yildirim, *J. Phys. Chem. C*, 2007, **111**, 16131-16137.

27. I. Senkovska and S. Kaskel, *Microporous Mesoporous Mater.*, 2008, **112**, 108-115.

28. K. Seki, *Chem. Commun.*, 2001, 1496-1497.

29. Y. Peng, V. Krungleviciute, I. Eryazici, J. T. Hupp, O. K. Farha and T. Yildirim, *J. Am. Chem. Soc.*, 2013, **135**, 11887-11894.

30. Y. He, W. Zhou, T. Yildirim and B. Chen, *Energy Environ. Sci.*, 2013, **6**, 2735-2744.

31. M. Tagliabue, C. Rizzo, R. Millini, P. D. C. Dietzel, R. Blom and S. Zanardi, *J. Porous Mater.*, 2011, **18**, 289-296.

32. Z. Jia, H. Li, Z. Yu, P. Wang and X. Fan, *Materials Lett.*, 2011, **65**, 2445-2447.

33. M. Kondo, T. Yoshitomi, K. Seki, H. Matsuzaka and S. Kitagawa, *Angew. Chem. Int. Ed.*, 1997, **36**, 1725-1727.

34. M. Eddaoudi, J. Kim, N. Rosi, D. Vodak, J. Wachter, M. O'Keeffe and O. M. Yaghi, *Science*, 2002, **295**, 469-472.

35. K. Seki, S. Takamizawa and W. Mori, *Chem. Lett.*, 2001, **30**, 332-333.

36. K. Seki and W. Mori, *J. Phys. Chem. B*, 2002, **106**, 1380-1385.

37. H. Kim, D. G. Samsonenko, S. Das, G.-H. Kim, H.-S. Lee, D. N. Dybtsev, E. A. Berdonosova and K. Kim, *Chem. Asian J.*, 2009, **4**, 886-891.

38. H. Wang, J. Getzschmann, I. Senkovska and S. Kaskel, *Microporous Mesoporous Mater.*, 2008, **116**, 653-657.

39. L.-G. Zhua and H.-P. Xiao, *Z. Anorg. Allg. Chem.*, 2008, **634**, 845-847.

40. K. Seki, *Phys. Chem. Chem. Phys.*, 2002, **4**, 1968-1971.

41. P. Chowdhury, S. Mekala, F. Dreisbach and S. Gumma, *Microporous Mesoporous Mater.*, 2012, **152**, 246-252.

42. A. D. Wiersum, J.-S. Chang, C. Serre and P. L. Llewellyn, *Langmuir*, 2013, **29**, 3301-3309.

43. J. Getzschmann, I. Senkovska, D. Wallacher, M. Tovar, D. Fairen-Jimenez, T. Düren, J. M. v. Baten, R. Krishna and S. Kaskel, *Microporous Mesoporous Mater.*, 2010, **136**, 50-58.

44. J. Moellmer, A. Moeller, F. Dreisbach, R. Glaeser and R. Staudt, *Microporous Mesoporous Mater.*, 2011, **138**, 140-148.

45. S. Cavenati, C. A. Grande and A. E. Rodrigues, *Ind. Eng. Chem. Res.*, 2008, **47**, 6333-6335.

46. Z. Xiang, Z. Hu, D. Cao, W. Yang, J. Lu, B. Han and W. Wang, *Angew. Chem. Int. Ed.*, 2011, **50**, 491-494.

47. P. D. C. Dietzel, V. Besikiotis and R. Blom, *J. Mater. Chem.*, 2009, **19**, 7362-7370.

48. H. Wu, W. Zhou and T. Yildirim, *J. Am. Chem. Soc.*, 2009, **131**, 4995-5000.

49. S. Ma, D. Sun, J. M. Simmons, C. D. Collier, D. Yuan and H.-C. Zhou, *J. Am. Chem. Soc.*, 2008, **130**, 1012-1016.

50. J. Y. Lee, L. Pan, X. Huang, T. J. Emge and J. Li, *Adv. Funct. Mater.*, 2011, **21**, 993-998.

51. Z. Lu, L. Du, K. Tang and J. Bai, *Cryst. Growth Des.*, 2013, **13**, 2252-2255.

52. C. E. Wilmer, M. Leaf, C. Y. Lee, O. K. Farha, B. G. Hauser, J. T. Hupp and R. Q. Snurr, *Nature Chem.*, 2012, **4**, 83-89.

53. Z. Guo, H. Wu, G. Srinivas, Y. Zhou, S. Xiang, Z. Chen, Y. Yang, W. Zhou, M. O'Keeffe and B. Chen, *Angew. Chem. Int. Ed.*, 2011, **50**, 3178-3181.

54. X.-S. Wang, S. Ma, K. Rauch, J. M. Simmons, D. Yuan, X. Wang, T. Yildirim, W. C. Cole, J. J. López, A. d. Meijere and H.-C. Zhou, *Chem. Mater.*, 2008, **20**, 3145-3152.

55. D. Liu, H. Wu, S. Wang, Z. Xie, J. Li and W. Lin, *Chem. Sci.*, 2012, **3**, 3032-3037.

56. D. Sun, S. Ma, J. M. Simmons, J.-R. Li, D. Yuan and H.-C. Zhou, *Chem. Commun.*, 2010, **46**, 1329-1331.

57. X. Rao, J. Cai, J. Yu, Y. He, C. Wu, W. Zhou, T. Yildirim, B. Chen and G. Qian, *Chem. Commun.*, 2013, **49**, 6719-6721.

58. R. D. Kennedy, V. Krungleviciute, D. J. Clingerman, J. E. Mondloch, Y. Peng, C. E. Wilmer, A. A. Sarjeant, R. Q. Snurr, J. T. Hupp, T. Yildirim, O. K. Farha and C. A. Mirkin, *Chem. Mater.*, 2013, **25**, 3539-3543.

59. P. Rallapalli, D. Patil, K. P. Prasanth, R. S. Somani, R. V. Jasra and H. C. Bajaj, *J. Porous Mater.*, 2010, **17**, 523-528.

60. S. Bourrelly, P. L. Llewellyn, C. Serre, F. Millange, T. Loiseau and G. Férey, *J. Am. Chem. Soc.*, 2005, **127**, 13519-13521.

61. C. E. Wilmer, O. K. Farha, T. Yildirim, I. Eryazici, V. Krungleviciute, A. A. Sarjeant, R. Q. Snurr and J. T. Hupp, *Energy Environ. Sci.*, 2013, **6**, 1158-1163.

62. B. Li, Z. Zhang, Y. Li, K. Yao, Y. Zhu, Z. Deng, F. Yang, X. Zhou, G. Li, H. Wu, N. Nijem, Y. J. Chabal, Z. Lai, Y. Han, Z. Shi, S. Feng and J. Li, *Angew. Chem. Int. Ed.*, 2012, **51**, 1412-1415.

63. X. Duan, J. Yu, J. Cai, Y. He, C. Wu, W. Zhou, T. Yildirim, Z. Zhang, S. Xiang, M. O'Keeffe, B. Chen and G. Qian, *Chem. Commun.*, 2013, **49**, 2043-2045.

64. G.-Q. Kong, Z.-D. Han, Y. He, S. Ou, W. Zhou, T. Yildirim, R. Krishna, C. Zou, B. Chen and C.-D. Wu, *Chem. Eur. J.*, 2013, **19**, 14886-14894.

65. Y. Wang, C. Tan, Z. Sun, Z. Xue, Q. Zhu, C. Shen, Y. Wen, S. Hu, Y. Wang, T. Sheng and X. Wu, *Chem. Eur. J.*, 2013, **19**, 10.1002/chem.201302541.

66. D. Zhao, D. Yuan, A. Yakovenko and H.-C. Zhou, *Chem. Commun.*, 2010, **46**, 4196-4198.

67. X. Zhao, D. Sun, S. Yuan, S. Feng, R. Cao, D. Yuan, S. Wang, J. Dou and D. Sun, *Inorg. Chem.*, 2012, **51**, 10350-10355.

68. Y. He, H. Furukawa, C. Wu, M. O'Keeffe, R. Krishna and B. Chen, *Chem. Commun.*, 2013, **49**, 6773-6775.

69. P. L. Llewellyn, S. Bourrelly, C. Serre, Y. Filinchuk and G. Férey, *Angew. Chem. Int. Ed.*, 2006, **45**, 7751-7754.

70. C. Tan, S. Yang, N. R. Champness, X. Lin, A. J. Blake, W. Lewis and M. Schröder, *Chem. Commun.*, 2011, **47**, 4487-4489.

71. Y. He, Z. Zhang, S. Xiang, H. Wu, F. R. Fronczek, W. Zhou, R. Krishna, M. O'Keeffe and B. Chen, *Chem. Eur. J.*, 2012, **18**, 1901-1904.

72. X. Liu, M. Park, S. Hong, M. Oh, J. W. Yoon, J.-S. Chang and M. S. Lah, *Inorg. Chem.*, 2009, **48**, 11507-11509.

73. Y. He, S. Xiang, Z. Zhang, S. Xiong, C. Wu, W. Zhou, T. Yildirim, R. Krishna and B. Chen, *J. Mater. Chem. A*, 2013, **1**, 2543-2551.

74. H. Furukawa, N. Ko, Y. B. Go, N. Aratani, S. B. Choi, E. Choi, A. Ö. Yazaydin, R. Q. Snurr, M. O'Keeffe, J. Kim and O. M. Yaghi, *Science*, 2010, **329**, 424-428.

75. Z. Wang, B. Zheng, H. Liu, X. Lin, X. Yu, P. Yi and R. Yun, *Cryst. Growth Des.*, 2013, **13**, 5001-5006.

76. W. Lu, D. Yuan, T. A. Makal, J.-R. Li and H.-C. Zhou, *Angew. Chem. Int. Ed.*, 2012, **51**, 1580-1584.

77. N. Klein, H. C. Hoffmann, A. Cadiau, J. Getzschmann, M. R. Lohe, S. Paasch, T. Heydenreich, K. Adil, I. Senkovska, E. Brunner and S. Kaskel, *J. Mater. Chem.*, 2012, **22**, 10303-10312.

78. Q. Yang, V. Guillerm, F. Ragon, A. D. Wiersum, P. L. Llewellyn, C. Zhong, T. Devic, C. Serre and G. Maurin, *Chem. Commun.*, 2012, **48**, 9831-9833.

79. L. Li, S. Tang, C. Wang, X. Lv, M. Jiang, H. Wu and X. Zhao, *Chem. Commun.*, 2013, **49**, 10.1039/C1033CC48275H.

80. P. L. Llewellyn, S. Bourrelly, C. Serre, A. Vimont, M. Daturi, L. Hamon, G. D. Weireld, J.-S. Chang, D.-Y. Hong, Y. K. Hwang, S. H. Jhung and G. Férey, *Langmuir*, 2008, **24**, 7245-7250.

81. J. S. Lee, S. H. Jhung, J. W. Yoon, Y. K. Hwang and J.-S. Chang, *J. Ind. Eng. Chem.*, 2009, **15**, 674-676.

82. P. Long, H. Wu, Q. Zhao, Y. Wang, J. Dong and J. Li, *Microporous Mesoporous Mater.*, 2011, **142**, 489-493.

83. J. Pang, F. Jiang, M. Wu, D. Yuan, K. Zhou, J. Qian, K. Su and M. Hong, *Chem. Commun.*, 2013, **49**, 10.1039/C1033CC48381A.

84. G. Barin, V. Krungleviciute, D. A. Gomez-Gualdron, A. A. Sarjeant, R. Q. Snurr, J. T. Hupp, T. Yildirim and O. K. Farha, *Chem. Mater.*, 2014, 10.1021/cm404155s.

85. Y. Peng, G. Srinivas, C. E. Wilmer, I. Eryazici, R. Q. Snurr, J. T. Hupp, T. Yildirim and O. K. Farha, *Chem. Commun.*, 2013, **49**, 2992-2994.

86. N. Klein, I. Senkovska, I. A. Baburin, R. Grünker, U. Stoeck, M. Schlichtenmayer, B. Streppel, U. Mueller, S. Leoni, M. Hirscher and S. Kaskel, *Chem. Eur. J.*, 2011, **17**, 13007-13016.

87. T. K. Prasad, D. H. Hong and M. P. Suh, *Chem. Eur. J.*, 2010, **16**, 14043-14050.

88. S.-i. Noro, R. Kitaura, M. Kondo, S. Kitagawa, T. Ishii, H. Matsuzaka and M. Yamashita, *J. Am. Chem. Soc.*, 2002, **124**, 2568-2583.

89. S.-i. Noro, S. Kitagawa, M. Kondo and K. Seki, *Angew. Chem. Int. Ed.*, 2000, **39**, 2082-2084.

90. L. Li, S. Tang, X. Lv, M. Jiang, C. Wang and X. Zhao, *New J. Chem.*, 2013, **37**, 3662-3670.

91. M. C. Das, H. Xu, Z. Wang, G. Srinivas, W. Zhou, Y.-F. Yue, V. N. Nesterov, G. Qian and B. Chen, *Chem. Commun.*, 2011, **47**, 11715-11717

92. I. Senkovska, F. Hoffmann, M. Fröba, J. Getzschmann, W. Böhlmann and S. Kaskel, *Microporous Mesoporous Mater.*, 2009, **122**, 93-98.

93. V. Bon, V. Senkovskyy, I. Senkovska and S. Kaskel, *Chem. Commun.*, 2012, **48**, 8407-8409.

94. Y.-N. Gong, M. Meng, D.-C. Zhong, Y.-L. Huang, L. Jiang and T.-B. Lu, *Chem. Commun.*, 2012, **48**, 12002-12004.

95. A. Santra, I. Senkovska, S. Kaskel and P. K. Bharadwaj, *Inorg. Chem.*, 2013, **52**, 7358-7366.

96. J. I. Feldblyum, D. Dutta, A. G. Wong-Foy, A. Dailly, J. Imirzian, D. W. Gidley and A. J. Matzger, *Langmuir*, 2013, **29**, 8146-8153.

97. D. Yuan, D. Zhao and H.-C. Zhou, *Inorg. Chem.*, 2011, **50**, 10528-10530.

98. U. Stoeck, S. Krause, V. Bon, I. Senkovska and S. Kaskel, *Chem. Commun.*, 2012, **48**, 10841-10843.

99. D. Han, F.-L. Jiang, M.-Y. Wu, L. Chen, Q.-H. Chen and M.-C. Hong, *Chem. Commun.*, 2011, **47**, 9861-9863.

100. C. Hou, Q. Liu, J. Fan, Y. Zhao, P. Wang and W.-Y. Sun, *Inorg. Chem.*, 2012, **51**, 8402-8408.

101. J. F. Eubank, H. Mouttaki, A. J. Cairns, Y. Belmabkhout, L. Wojtas, R. Luebke, M. Alkordi and M. Eddaoudi, *J. Am. Chem. Soc.*, 2011, **133**, 14204-14207.

102. T. K. Prasad and M. P. Suh, *Chem. Eur. J.*, 2012, **18**, 8673-8680.

103. Y. Yan, S. Yang, A. J. Blake, W. Lewis, E. Poirier, S. A. Barnett, N. R. Champness and M. Schröder, *Chem. Commun.*, 2011, **47**, 9995-9997.

104. M. K. Sharma, I. Senkovska, S. Kaskel and P. K. Bharadwaj, *Inorg. Chem.*, 2011, **50**, 539-544.

105. N. Klein, I. Senkovska, K. Gedrich, U. Stoeck, A. Henschel, U. Mueller and S. Kaskel, *Angew. Chem. Int. Ed.*, 2009, **48**, 9954-9957.

106. W.-Y. Gao, R. Cai, L. Meng, L. Wojtas, W. Zhou, T. Yildirim, X. Shi and S. Ma, *Chem. Commun.*, 2013, **49**, 10516-10518.

107. K. Gedrich, I. Senkovska, N. Klein, U. Stoeck, A. Henschel, M. R. Lohe, I. A. Baburin, U. Mueller and S. Kaskel, *Angew. Chem. Int. Ed.*, 2010, **49**, 8489-8492.

108. B. Zheng, R. Yun, J. Bai, Z. Lu, L. Du and Y. Li, *Inorg. Chem.*, 2013, **52**, 2823-2829.

109. M. Xue, Y. Liu, R. M. Schaffino, S. Xiang, X. Zhao, Guang-Shan Zhu, S.-L. Qiu and B. Chen, *Inorg. Chem.*, 2009, **48**, 4649-4651.

110.   J. Cai, X. Rao, Y. He, J. Yu, C. Wu, W. Zhou, T. Yildirim, B. Chen and G. Qian, *Chem. Commun.*, 2013, **49**, 10.1039/c1033cc48747d.

111.   R. Grünker, I. Senkovska, R. Biedermann, N. Klein, M. R. Lohe, P. M. ller and S. Kaskel, *Chem. Commun.*, 2011, **47**, 490-492.

112.   Z. Wang, B. Zheng, H. Liu, P. Yi, X. Li, X. Yu and R. Yun, *Dalton Trans.*, 2013, **42**, 11304-11311.

113.   B. Zheng, Z. Yang, J. Bai, Y. Li and S. Li, *Chem. Commun.*, 2012, **48**, 7025-7027.

114.   X. Zhao, X. Wang, S. Wang, J. Dou, P. Cui, Z. Chen, D. Sun, X. Wang and D. Sun, *Cryst. Growth Des.*, 2012, **12**, 2736-2739.

115.   R. Kitaura, K. Seki, G. Akiyama and S. Kitagawa, *Angew. Chem. Int. Ed.*, 2003, **42**, 428-431.

116.   Y. He, Z. Guo, S. Xiang, Z. Zhang, W. Zhou, F. R. Fronczek, S. Parkin, S. T. Hyde, M. O'Keeffe and B. Chen, *Inorg. Chem.*, 2013, **52**, 11580-11584.

117.   X. Lv, S. Tang, L. Li, J. Cai, C. Wang, X. Xu and X. Zhao, *Eur. J. Inorg. Chem.*, 2013, 5081-5085.

118.   T. Loiseau, L. Lecroq, C. Volkringer, J. Marrot, G. Férey, M. Haouas, F. Taulelle, S. Bourrelly, P. L. Llewellyn and M. Latroche, *J. Am. Chem. Soc.*, 2006, **128**, 10223-10230.

119.   D. Tian, Q. Chen, Y. Li, Y.-H. Zhang, Z. Chang and X.-H. Bu, *Angew. Chem. Int. Ed.*, 2013, 10.1002/anie.201307681.

120.   M. Kondo, M. Shimamura, S.-i. Noro, S. Minakoshi, A. Asami, K. Seki and S. Kitagawa, *Chem. Mater.*, 2000, **12**, 1288-1299.

121.   Z. Guo, R. Cao, X. Wang, Hongfang Li, W. Yuan, G. Wang, H. Wu and J. Li, *J. Am. Chem. Soc.*, 2009, **131**, 6894-6895.

122.   M. Kondo, T. Okubo, A. Asami, S.-i. Noro, T. Yoshitomi, S. Kitagawa, T. Ishii, H. Matsuzaka and K. Seki, *Angew. Chem. Int. Ed.*, 1999, **38**, 140-143.

123.   H. J. Park, Y. E. Cheon and M. P. Suh, *Chem. Eur. J.*, 2010, **16**, 11662-11669.

124.   E. Barea, G. Tagliabue, W.-G. Wang, M. Pérez-Mendoza, L. Mendez-Liñan, F. J. López-Garzon, S. Galli, N. Masciocchi and J. A. R. Navarro, *Chem. Eur. J.*, 2010, **16**, 931-937.

125.   M. Anbia and S. Sheykhi, *J. Nat. Gas Chem.*, 2012, **21**, 680-684.

126.   P. L. Llewellyn, S. Bourrelly, C. Vagner, N. Heymans, H. Leclerc, A. Ghoufi, P. Bazin, A. Vimont, M. Daturi, T. Devic, C. Serre, G. D. Weireld and G. Maurin, *J. Phys. Chem. C*, 2013, **117**, 962-970.

127.   K. Seki, S. Takamizawa and W. Mori, *Chem. Lett.*, 2001, **30**, 122-123.

128.   D. N. Dybtsev, H. Chun and K. Kim, *Angew. Chem. Int. Ed.*, 2004, **43**, 5033-5036.

129.   T. Düren, L. Sarkisov, O. M. Yaghi and R. Q. Snurr, *Langmuir*, 2004, **20**, 2683-2689.

130.   S. Ma, X.-S. Wang, C. D. Collier, E. S. Manis and H.-C. Zhou, *Inorg. Chem.*, 2007, **46**, 8499-8501.

131.   H. Wu, W. Zhou and T. Yildirim, *J. Phys. Chem. C*, 2009, **113**, 3029-3035.

132.   D. Y. Siberio-Pérez, A. G. Wong-Foy, O. M. Yaghi and A. J. Matzger, *Chem. Mater.*, 2007, **19**, 3681-3685.

133.   H. K. Chae, D. Y. Siberio-Pérez, J. Kim, Y. Go, M. Eddaoudi, A. J. Matzger, M. O'Keeffe and O. M. Yaghi, *Nature*, 2004, **427**, 523-527.

134.   K. Koh, A. G. Wong-Foy and A. J. Matzger, *Angew. Chem. Int. Ed.*, 2008, **47**, 677-680.

135.   K. Koh, A. G. Wong-Foy and A. J. Matzger, *J. Am. Chem. Soc.*, 2009, **131**, 4184-4185.

136.   N. L. Rosi, J. Kim, M. Eddaoudi, B. Chen, M. O'Keeffe and O. M. Yaghi, *J. Am. Chem. Soc.*, 2005, **127**, 1504-1518.

137.   P. D. C. Dietzel, Y. Morita, R. Blom and H. Fjellvåg, *Angew. Chem. Int. Ed.*, 2005, **44**, 6354-6358.

138.   P. D. C. Dietzel, B. Panella, M. Hirscher, R. Blom and H. Fjellvåg, *Chem. Commun.*, 2006, 959-961.

139.   P. D. C. Dietzel, R. Blom and H. Fjellvåg, *Eur. J. Inorg. Chem.*, 2008, 3624-3632.

140.   S. R. Caskey, A. G. Wong-Foy and A. J. Matzger, *J. Am. Chem. Soc.*, 2008, **130**, 10870-10871.

141.   W. Zhou, H. Wu and T. Yildirim, *J. Am. Chem. Soc.*, 2008, **130**, 15268-15269.

142.   S. Xiang, W. Zhou, Z. Zhang, M. A. Green, Y. Liu and B. Chen, *Angew. Chem. Int. Ed.*, 2010, **49**, 4615-4618.

143.   E. D. Bloch, W. L. Queen, R. Krishna, J. M. Zadrozny, C. M. Brown and J. R. Long, *Science*, 2012, **335**, 1606-1610.

144.   P. D. C. Dietzel, R. E. Johnsen, H. Fjellvåg, S. Bordiga, E. Groppo, S. Chavan and R. Blom, *Chem. Commun.*, 2008, 5125-5127.

145.   M. K. Rana, H. S. Koh, H. Zuberi and D. J. Siegel, *J. Phys. Chem. C*, 2014, **118**, 2929-2942.

146.   S. S.-Y. Chui, S. M.-F. Lo, J. P. H. Charmant, A. G. Orpen and I. D. Williams, *Science*, 1999, **283**, 1148-1150.

147.   H. Wu, J. M. Simmons, Y. Liu, C. M. Brown, X.-S. Wang, S. Ma, V. K. Peterson, P. D. Southon, C. J. Kepert, H.-C. Zhou, T. Yildirim and W. Zhou, *Chem. Eur. J.*, 2010, **16**, 5205-5214.

148.   A. P. Nelson, O. K. Farha, K. L. Mulfort and J. T. Hupp, *J. Am. Chem. Soc.*, 2009, **131**, 458-460.

149.   L. Ma, A. Jin, Z. Xie and W. Lin, *Angew. Chem. Int. Ed.*, 2009, **48**, 9905-9908.

150.   B. Chen, N. W. Ockwig, A. R. Millward, D. S. Contreras and O. M. Yaghi, *Angew. Chem. Int. Ed.*, 2005, **44**, 4745-4749.

151.   X. Lin, J. Jia, X. Zhao, K. M. Thomas, A. J. Blake, G. S. Walker, N. R. Champness, P. Hubberstey and M. Schröder, *Angew. Chem. Int. Ed.*, 2006, **45**, 7358-7364.

152.   X. Lin, I. Telepeni, A. J. Blake, A. Dailly, C. M. Brown, J. M. Simmons, M. Zoppi, G. S. Walker, K. M. Thomas, T. J. Mays, P. Hubberstey, N. R. Champness and M. Schröder, *J. Am. Chem. Soc.*, 2009, **131**, 2159-2171.

153.   Y. Hu, S. Xiang, W. Zhang, Z. Zhang, L. Wang, J. Bai and B. Chen, *Chem. Commun.*, 2009, 7551-7553.

154.   S. Yang, X. Lin, A. Dailly, A. J. Blake, P. Hubberstey, N. R. Champness and M. Schröder, *Chem. Eur. J.*, 2009, **15**, 4829-4835.

155.   S. M. P. Lucena, P. G. M. Mileo, P. F. G. Silvino and J. Cério L. Cavalcante, *J. Am. Chem. Soc.*, 2011, **133**, 19282-19285.

156.   Y. He, R. Krishna and B. Chen, *Energy Environ. Sci.*, 2012, **5**, 9107-9120

157.   D. Yuan, D. Zhao, D. Sun and H.-C. Zhou, *Angew. Chem. Int. Ed.*, 2010, **49**, 5357-5361.

158.   S. Hong, M. Oh, M. Park, J. W. Yoon, J.-S. Chang and M. S. Lah, *Chem. Commun.*, 2009, 5397-5399.

159. Y. Yan, X. Lin, S. Yang, A. J. Blake, A. Dailly, N. R. Champness, P. Hubbberstey and M. Schröder, *Chem. Commun.*, 2009, 1025-1027.

160. O. K. Farha, C. E. Wilmer, I. Eryazici, B. G. Hauser, P. A. Parilla, K. O'Neill, A. A. Sarjeant, S. T. Nguyen, R. Q. Snurr and J. T. Hupp, *J. Am. Chem. Soc.*, 2012, **134**, 9860-9863.

161. Y. Yan, I. Telepeni, S. Yang, X. Lin, W. Kockelmann, A. Dailly, A. J. Blake, W. Lewis, G. S. Walker, D. R. Allan, S. A. Barnett, N. R. Champness and M. Schröder, *J. Am. Chem. Soc.*, 2010, **132**, 4092-4094.

162. D. Zhao, D. Yuan, D. Sun and H.-C. Zhou, *J. Am. Chem. Soc.*, 2009, **131**, 9186-9188.

163. B. Zheng, J. Bai, J. Duan, L. Wojtas and M. J. Zaworotko, *J. Am. Chem. Soc.*, 2011, **133**, 748-751.

164. X.-J. Wang, P.-Z. Li, Y. Chen, Q. Zhang, H. Zhang, X. X. Chan, R. Ganguly, Y. Li, J. Jiang and Y. Zhao, *Sci. Rep.*, 2013, **3**, 1149.

165. J. F. Eubank, F. Nouar, R. Luebke, A. J. Cairns, L. Wojtas, M. Alkordi, T. Bousquet, M. R. Hight, J. Eckert, J. P. Embs, P. A. Georgiev and M. Eddaoudi, *Angew. Chem. Int. Ed.*, 2012, **51**, 10099-10103.

166. O. K. Farha, A. Ö. Yazaydın, I. Eryazici, C. D. Malliakas, B. G. Hauser, M. G. Kanatzidis, S. T. Nguyen, R. Q. Snurr and J. T. Hupp, *Nature Chem.*, 2010, **2**, 944-948.

167. F. Nouar, J. F. Eubank, T. Bousquet, L. Wojtas, M. J. Zaworotko and M. Eddaoudi, *J. Am. Chem. Soc.*, 2008, **130**, 1833-1835.

168. O. K. Farha, I. Eryazici, N. C. Jeong, B. G. Hauser, C. E. Wilmer, A. A. Sarjeant, R. Q. Snurr, S. T. Nguyen, A. Ö. Yazaydın and J. T. Hupp, *J. Am. Chem. Soc.*, 2012, **134**, 15016-15021.

169. G. Férey, C. Serre, C. Mellot-Draznieks, FranckMillange, S. Surblé, J. Dutour and I. Margiolaki, *Angew. Chem. Int. Ed.*, 2004, **43**, 6296-6301.

170. G. Férey, C. Mellot-Draznieks, C. Serre, F. Millange, J. Dutour, S. Surblé and I. Margiolaki, *Science*, 2005, **309**, 2040-2042.

171. F. Millange, C. Serre and G. Férey, *Chem. Commun.*, 2002, 822-823.

172. J. H. Cavka, S. Jakobsen, U. Olsbye, N. Guillou, C. Lamberti, S. Bordiga and K. P. Lillerud, *J. Am. Chem. Soc.*, 2008, **130**, 13850-13851.

173. H. Wu, Y. S. Chua, V. Krungleviciute, M. Tyagi, P. Chen, T. Yildirim and W. Zhou, *J. Am. Chem. Soc.*, 2013, **135**, 10525-10532.

174. J. Lan, D. Cao and W. Wang, *Langmuir*, 2010, **26**, 220-226.

175. http://www.basf.com/group/corporate/us/en/news-and-media-relations/news-releases/news-releases-usa/P-13-452

TOC Figure

Porous metal-organic frameworks have been emerging as very promising materials for methane (natural gas) storage.

This journal is © The Royal Society of Chemistry 2012

Chem. Soc. Rev., 2012, **00**, 1-3 | **23**